2. IR SPECTROSCOPY

Advantages: Simple
Cheap
Sensitive
Good spectral resolution
Flexibility

Surfaces: homogeneous (polymers)
supported thin films
adsorbed species

on single crystal on supported catalysts

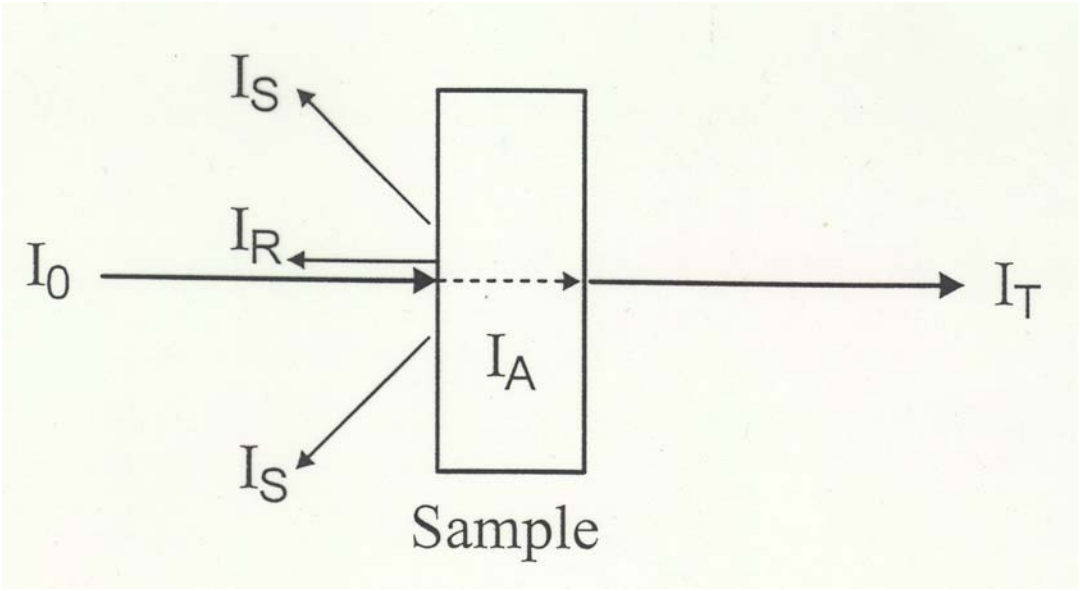

$$I_0 = I_A + I_T + I_R + I_S$$

For several decades infrared spectroscopy has been a very important tool for study of catalyst properties, catalytic processes and adsorbed species on catalyst

surfaces. Especially the today's FTIR techniques have a number of significant intrinsic advantages due to the high signal-to-noise ratio, the high sensitivity, the fast scanning speed and fast computation and the latest developments of FTIR microscopy. Not only the above advantages of FTIR spectrometers but also the implementation of more and more convenient techniques continues to make a significant impact on the study of catalysts and catalytic processes. The most important of these techniques are the diffuse reflectance (DRIFT), the emission (IRES), the photoacoustic (PA), the FTIR microscopy and the time resolved (picoseconds) FTIR spectroscopy. In spite of the special advantages of the above listed techniques the conventional transmission spectroscopy is still the most popular FTIR technique used for catalysis studies.

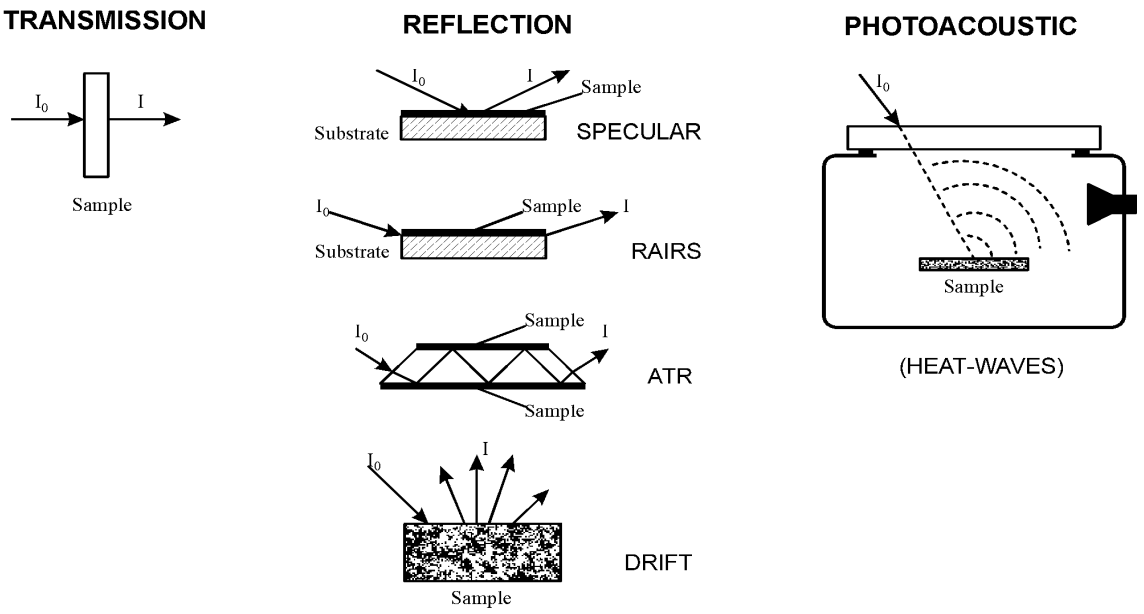

The most common IR techniques used for surface studies.

Excitation by radiation

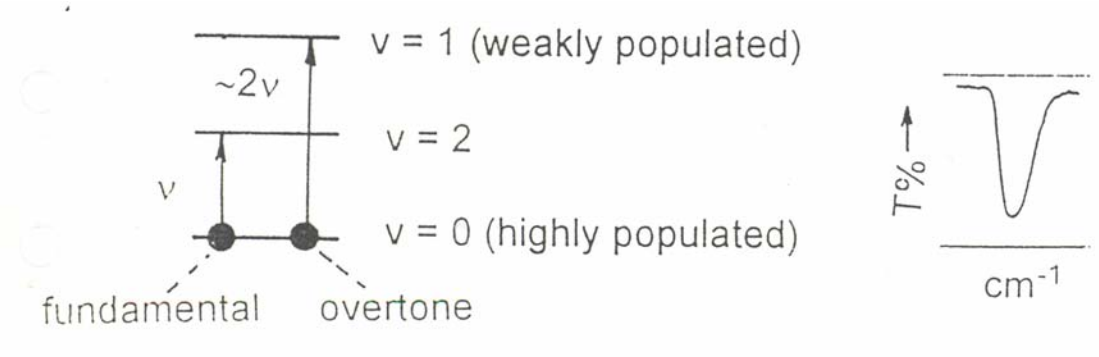

2.1. TRANSMISSION TECHNIQUES

There are several FTIR spectroscopic methods for study adsorbed molecules on catalysts. Infrared transmission spectroscopy is still dominantly used as most convenient and traditional technique for powdered samples. There are several advantages to study supported metal catalysts or metal oxide catalysts because beside their high specific area they relate to real industrial catalysts and they can press into self supporting pellets which are partially transparent.
The pressed pellets have to put into an *in situ* catalytic cell, for pre treatment and study the chemical process and chemisorbed species.

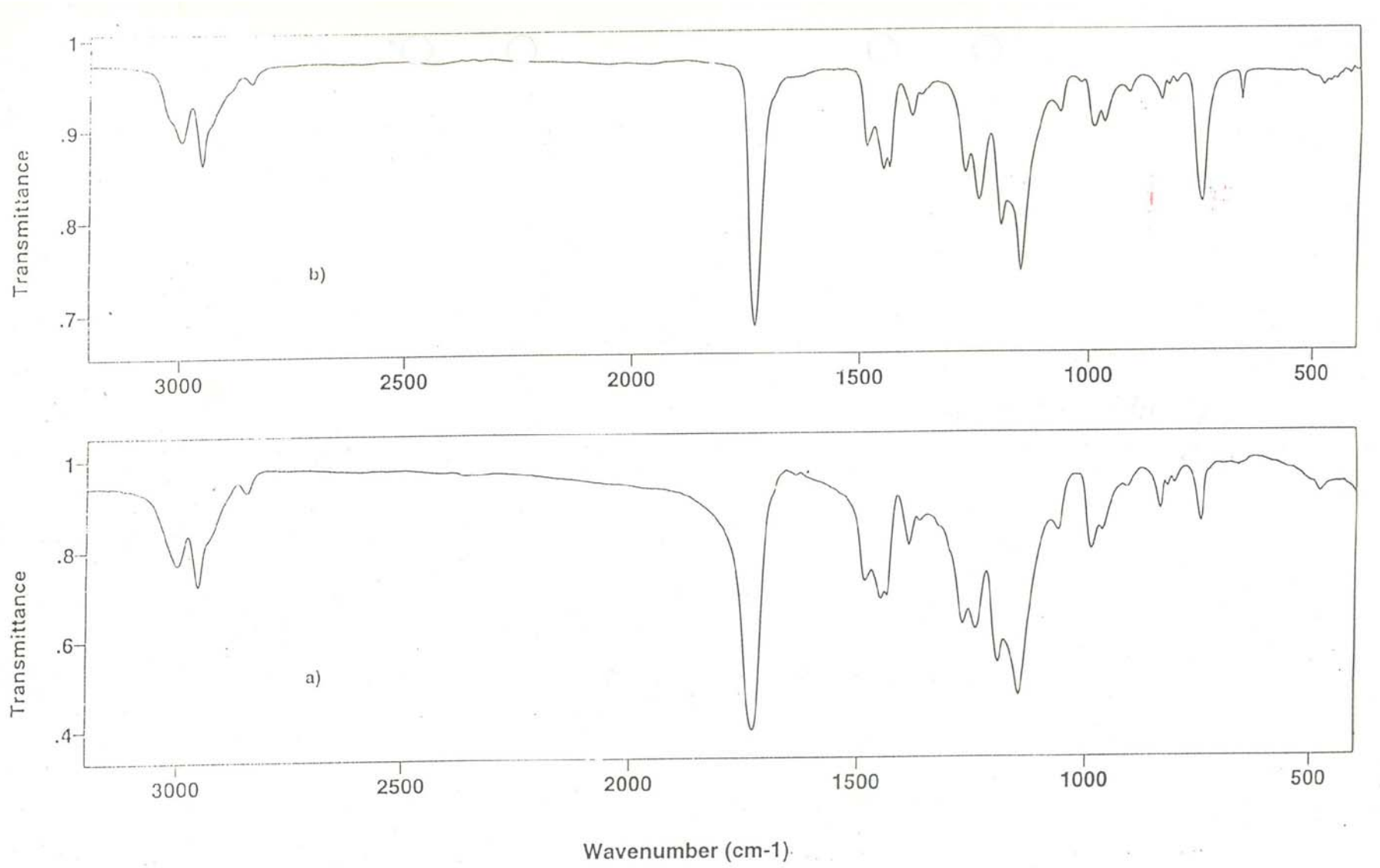

IR transmission spectra of PMMA: (a) east film on KBr window,
(b) KBr pellet of PMMA saw-dust

Transmission catalytic cells

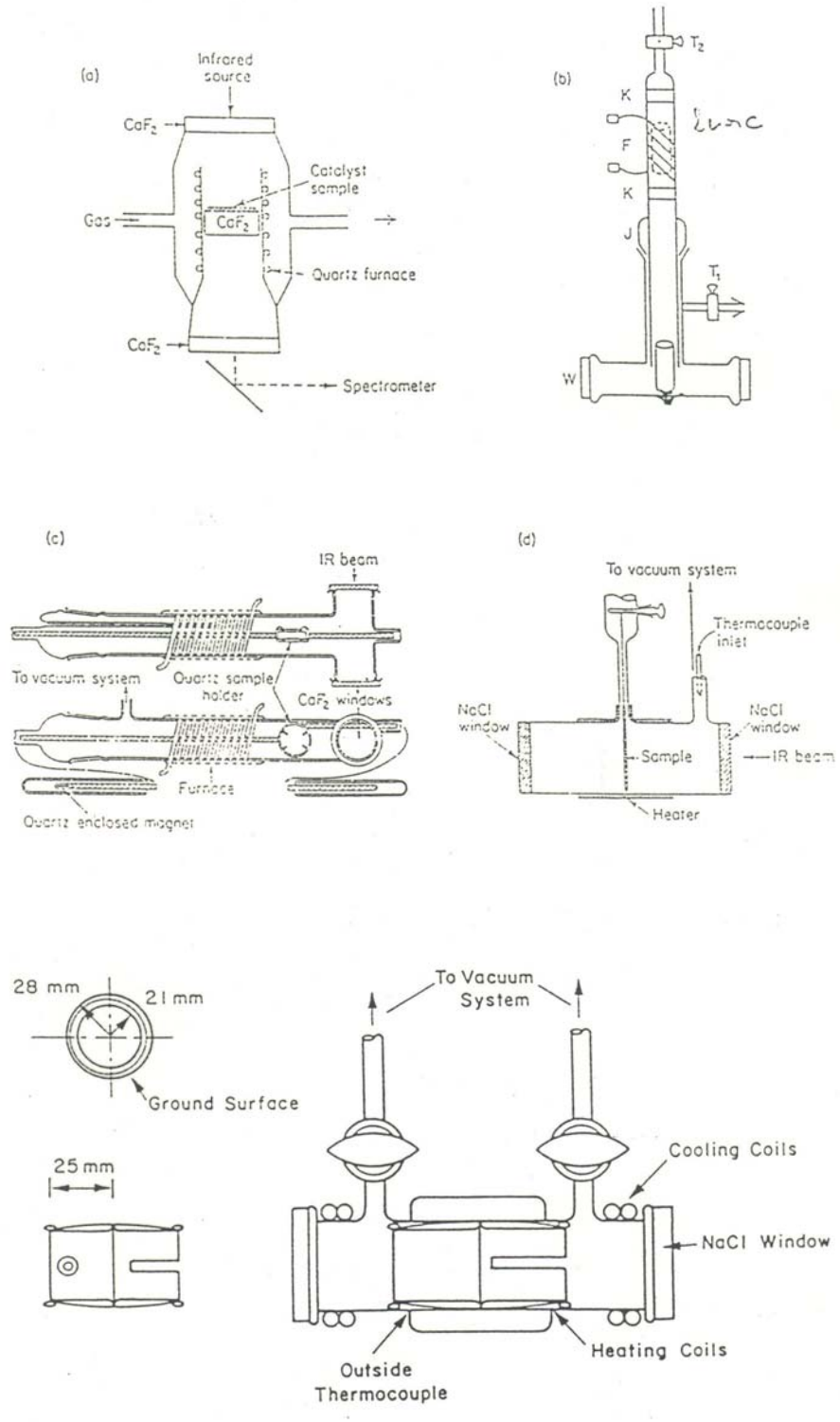

Infrared cell and sample holder

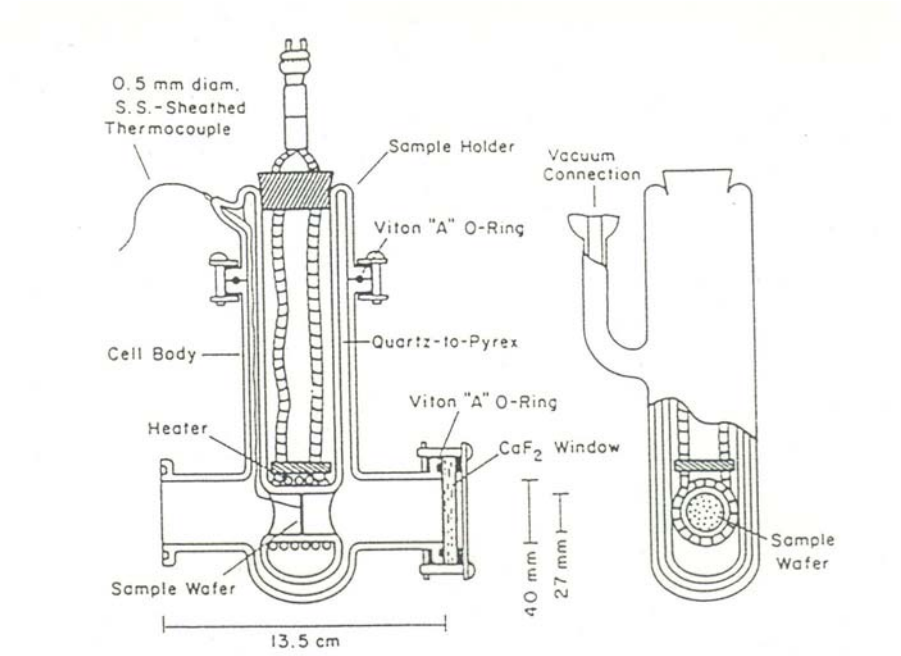

Infrared cell for catalyst studies

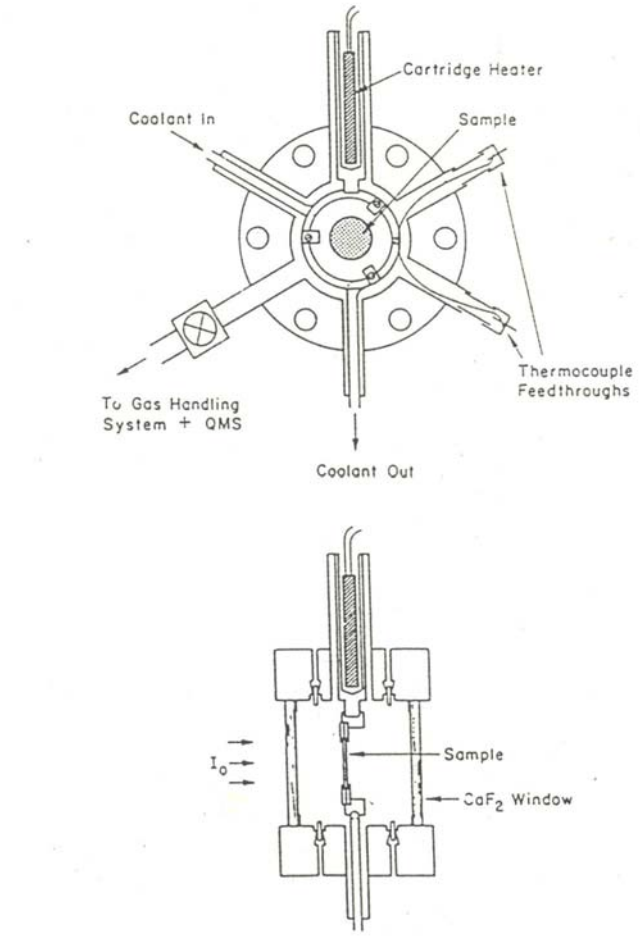

UHV cell for simultaneous infrared and thermal desorption spectroscopy

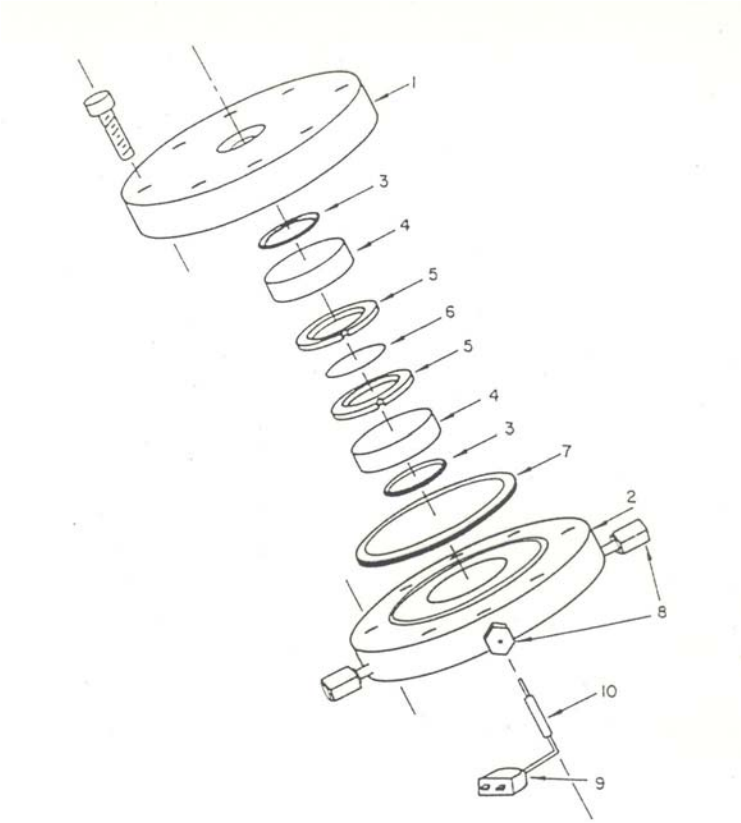

High pressure infrared cell:

1. top flange; 2. bottom flange; 3. Kalrez O-ring; 4. CaF_2 window; 5. sample holder; 6. catalyst disk; 7. copper gasket; 8. Swagelok fitting; 9. heated thermocouple; 10. sleeve attached to thermocouple sleeve

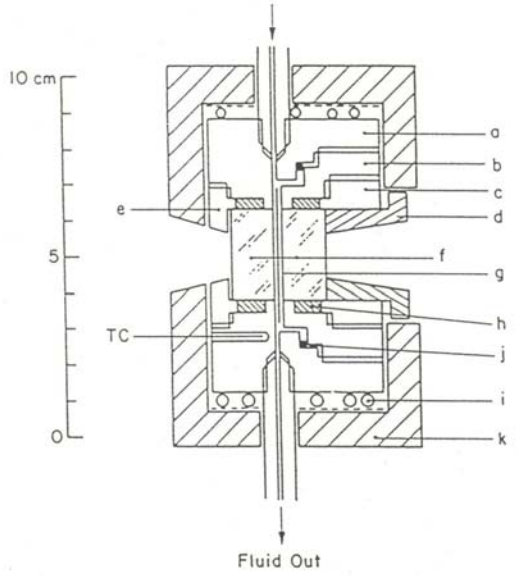

High pressure infrared cell:

a. reactor body; b. removable side of the reaction space; c. window seal compression plug; d. adjustable window support; e. window support/seal compression plug; f. optical windows; g. catalyst disk in reaction space; h. window seal; i. heating element; j. O-ring; k. thermal insulation box

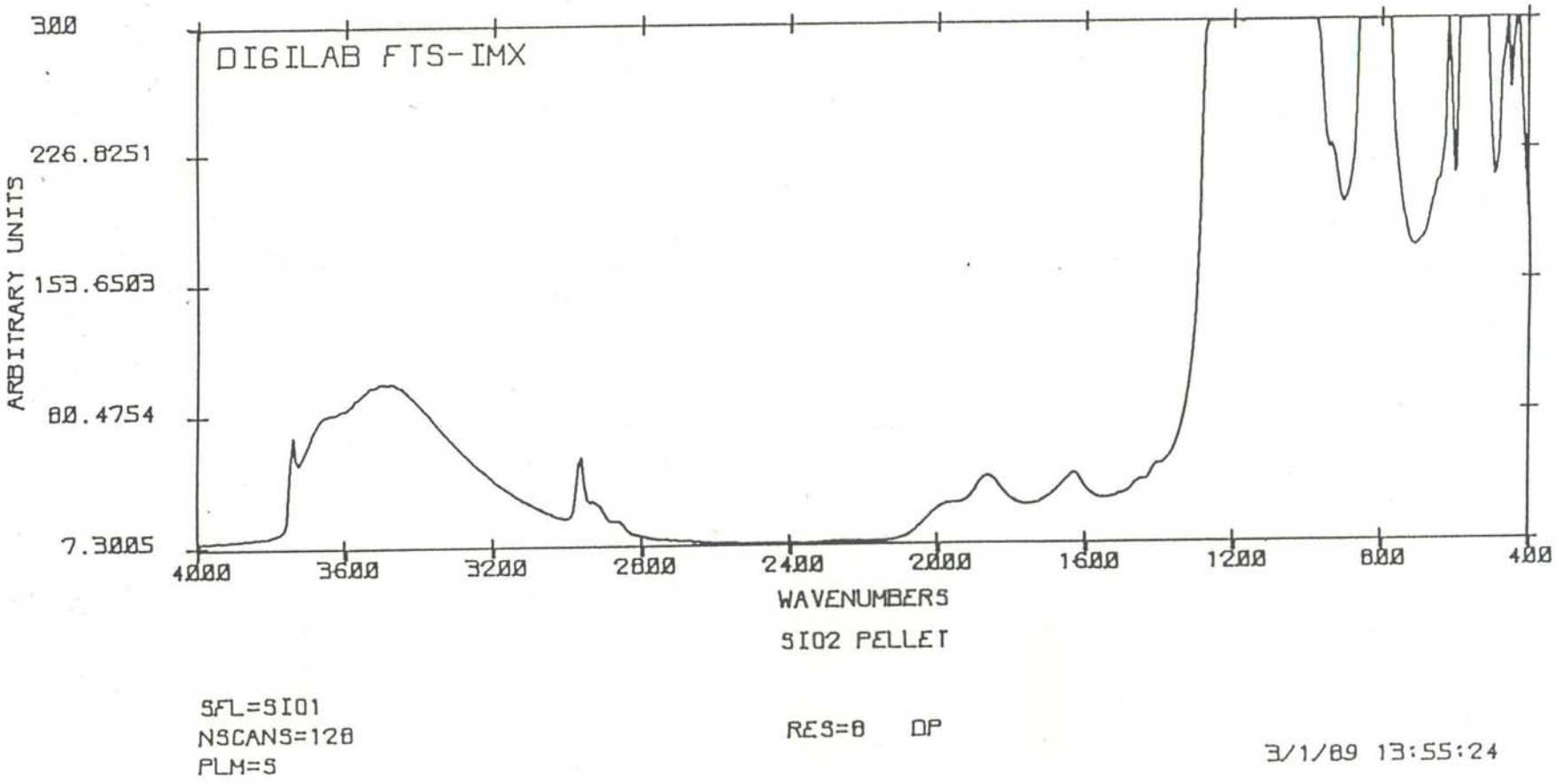
DIGILAB FTS-IMX
300
226.8251
153.6503
80.4754
7.3005
ARBITRARY UNITS
4000
3600
3200
2800
2400
2000
1600
1200
800
400
WAVENUMBERS
SIO2 PELLET
SFL=SI01
NSCANS=128
PLM=S
RES=8 DP
3/1/89 13:55:24

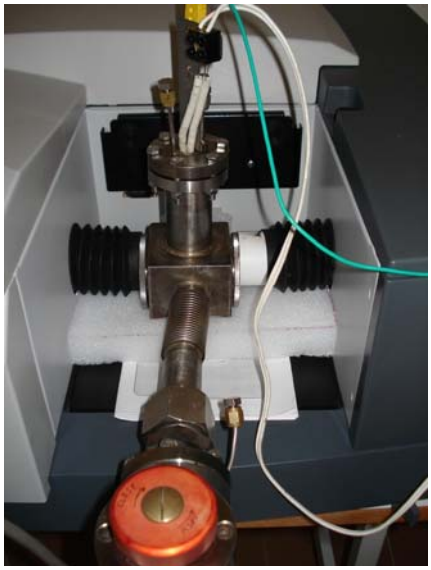

Variable temperature (-190- 450 ^{o}C) cell for *in situ* study of catalysts.

Both the temperature and the pressure can be varied and controlled. There are some specially constructed transmission cells operating as high temperature as 1273K and as high pressure as 100 MPa.
Transmission spectroscopy has some serious disadvantages:
a.) The self supporting pellets of the catalysts are usually opaque in the region below 1200-1300 cm^{-1}, therefore the most part of the fingerprint region is not detectable;
b.) Strong water and gas phase interference;
c.) Incapable of black materials (carbon, metal blacks etc.);
d.) Blackbody radiation of the sample a problem for high temperature study.

Determine the type of CO bonding on metal single crystals.

Substrate	νM-C(cm^{-1})	νCO(cm^{-1})	Type of bonding
Fe(110)	455	1890	
Ni(100)	480	2065	
	360	1930	
Ni(111)	400	1810	
Cu(100)	340	2090	
Ru(001)	445	1990	
Rh(111)	480	1990	
Pt(111)	480	2105	
	380	1870	
W(100)	365	2080	

Influence of the metal charge on CO stretching frequencies (cm^{-1})

Cations	Neutral molecules	Anions	
	$Ni(CO)_4$ 2057	$Co(CO)_4^-$ 1888	$Fe(CO)_4^{2-}$ 1786
	$Fe(CO)_5$ 2034 2014	$Mn(CO)_5^-$ 1895 1863	
$Mn(CO)_6^+$ 2090	$Cr(CO)_6$ 1981	$V(CO)_6^-$ 1859	

Chemisorbed of hydrogen

Molecule	Raman frequency (cm^{-1})
H_2	4164
HD	3632
D_2	2993
H_2/porous glas	4131

Metal complexes of dihydrogen

Pd vapour + H_2 →

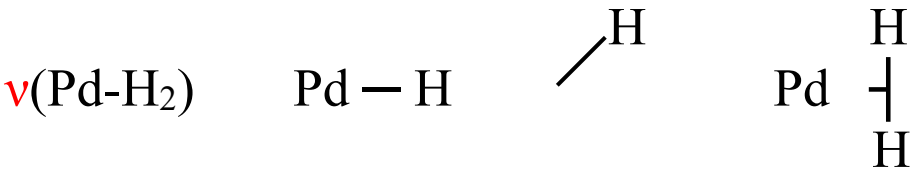

IR: 771 cm^{-1} 886,895 cm^{-1}

End – on Side – on

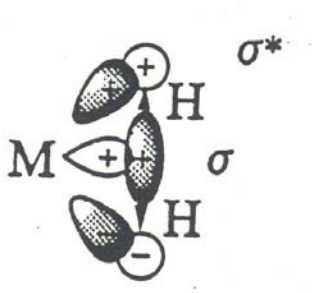

- σ – donation to metal
- back donation to σ* orbital

Hydrido complexes

M—H Frequencies of Hydrido Complexes (cm^{-1})

Complex	ν(MH)	δ(MH)
trans,trans-$[Cr(H)(CO)_2(NO)(PEt_3)_2]$	1661	—
$[Mo(H)(CN)_7]^{4-}$	1805	—
cis-$[Fe(H)(CO)_3P(OC_6H_5)_3]^-$	1895	—
trans-$[Fe(H)Cl\{C_2H_4(PEt_2)_2\}_2]$	1849	656
$[Co(H)(CN)_5]^{3-}$	1840	774
$[Rh(H)(CN)_5]^{3-}$	1980	781
$[Ir(H)(CN)_5]^{3-}$	2040	811
$Ir(H)(COD)\{As(C_6H_5)_3\}_2$ [a]	2030	—

[a] COD: 1,5-cyclooctadiene.

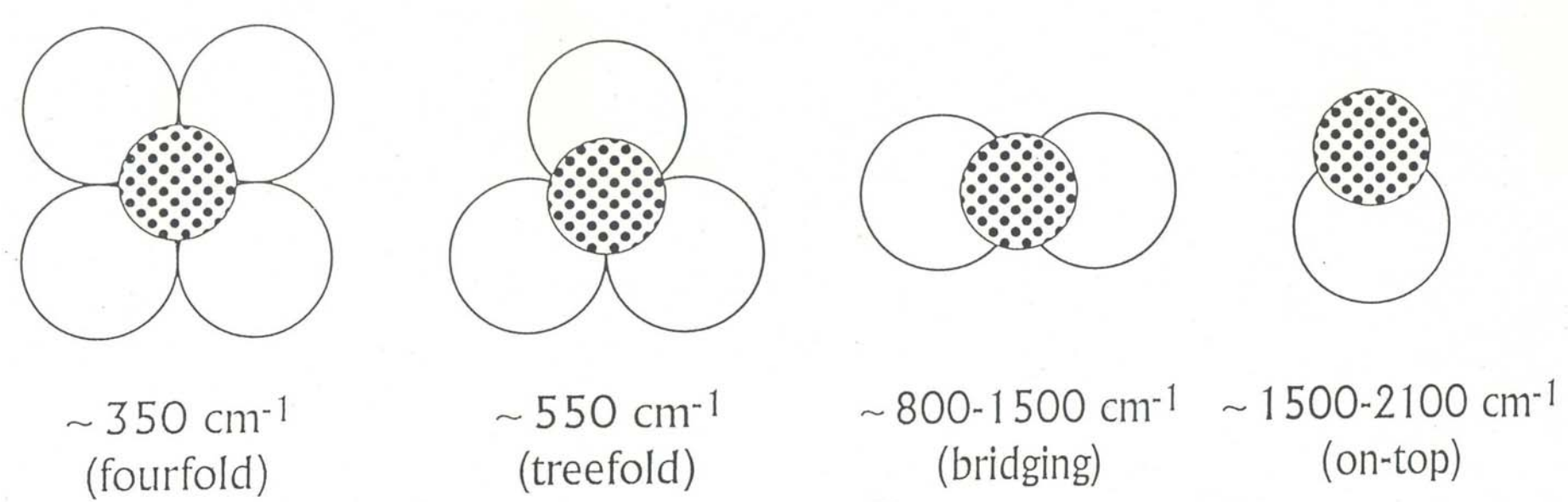

Frequency of the perpendicular metal-hydrogen stretching vibration in different sites.
CO chemisorption

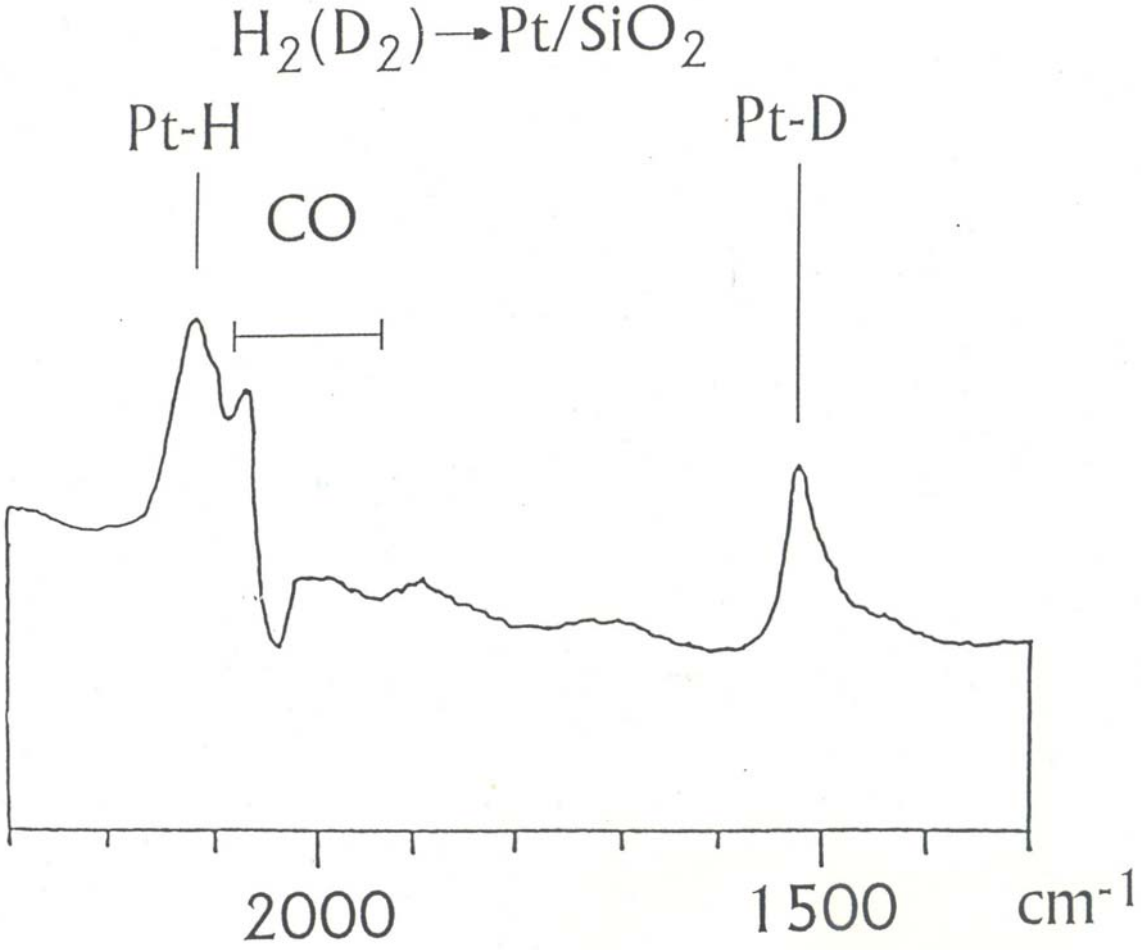

IR spectrum of 1:1 H_2 + D_2 mixture adsorbed on CO contaminated Pt/SiO_2
Pressure: 300 Pa

Platinum-Hydrogen Stretching Frequencies and Calculated Force Constants

Compound	ν(PtH) (cm^{-1})	ν(PtD) (cm^{-1})	K(PtH) (Ncm^{-1})	Remarks
Pt/SiO_2 (+H_2 300Pa)	2129	1526*	2.62	(a)
	2118	1519*	2.59	(a)
	2097	1504*	2.54	(a)
trans-[PtH(OCN)(PEt_3)$_2$]	2234	1589	2.93	(b)
trans-[PtHCl(PEt_3)$_2$]	2230	1610	2.83	(b)
trans-[PtH(NCS)(PEt_3)$_2$]	2195	1571	2.79	(b)
trans-[PtH(CN)(PEt_3)$_2$]	2072	1504	2.41	(b)

*Predicted (calculated) band components of the asymmetric shape experimental band at 1520 cm^{-1}

(a) This work.

(b) Experimental frequencies are taken from [16].

CO chemisorption
Type of bonding:

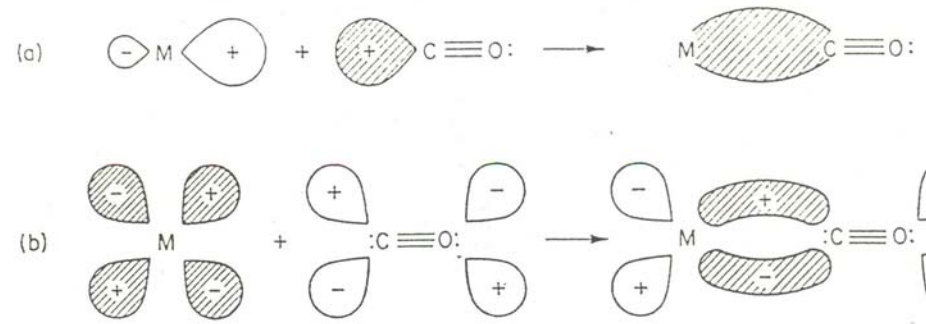

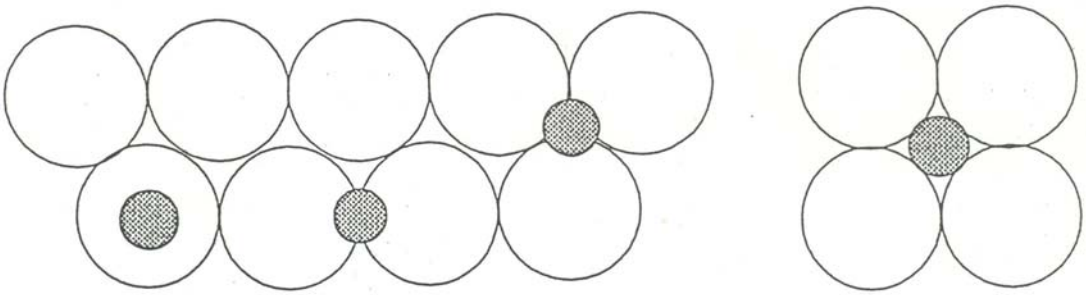

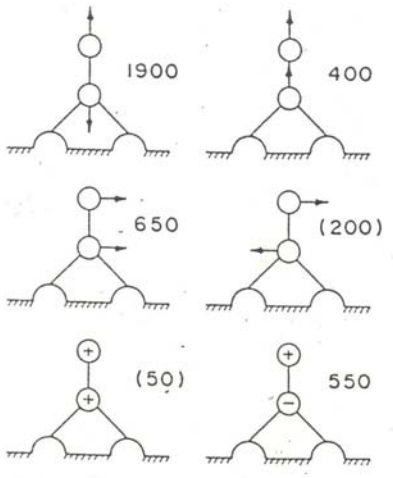

Infrared spectroscopy

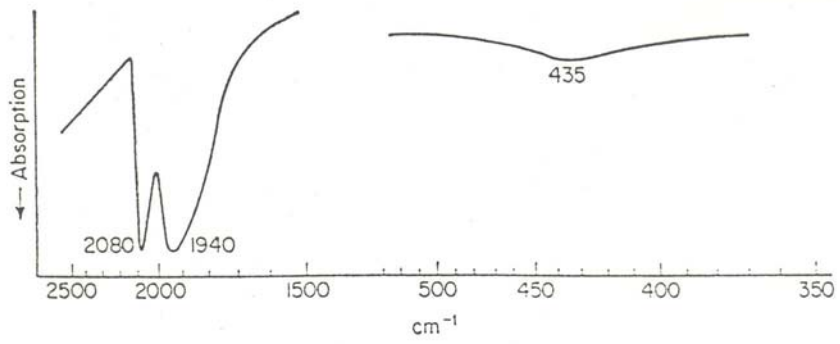

Infrared spectrum of CO chemisorbed on nickel

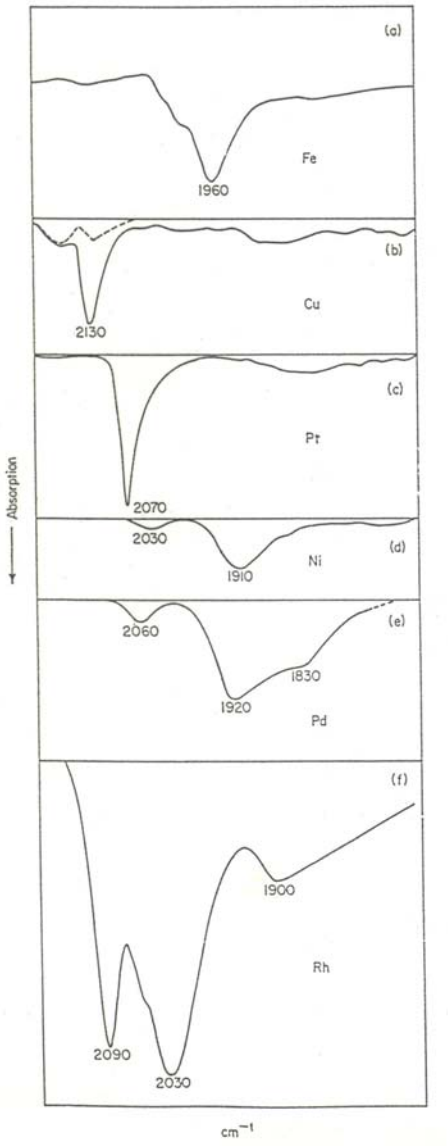

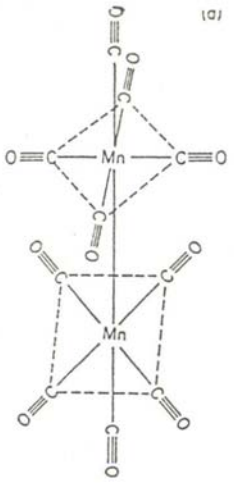

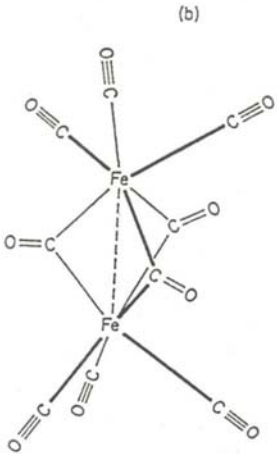

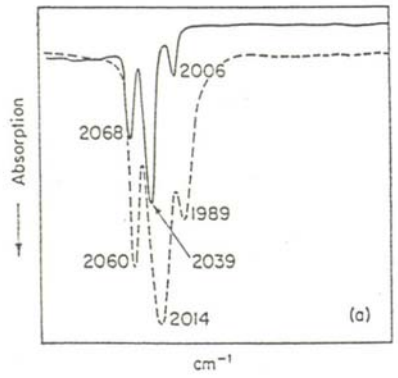

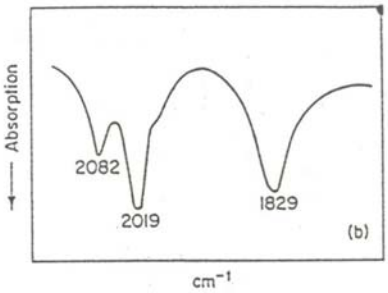

IR spectra of the above complexes

Metal carbonyl	Terminal	Bridge-bonding
$Ni(CO)_4$	2050, 2043	
$Fe(CO)_5$	2028, 1994	
$Cr(CO)_6$	2000	
$Mo(CO)_6$	2000	
$W(CO)_6$	1997	
$Co_2(CO)_8$	2077, 2054, 2034	1859
$Fe_2(CO)_9$	2080, 2034	1828

Supported metal catalysts: CO bands (cm^{-1}) Intensity s=strong; m=medium; w=weak			
Cu/SiO_2	2120 s	1830 w	
Ni/SiO_2	2030w	1950 s	
Pd/SiO_2	2050 w	1920	
Ru/Al_2O_2	2110 s, 2040s	2045 s	1925 m

CO adsorption on TiO_2 (anatase) surface

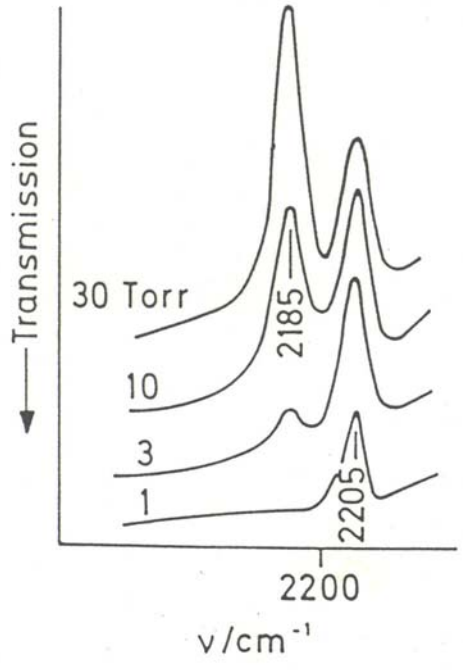

2.2 SPECULAR REFLECTION

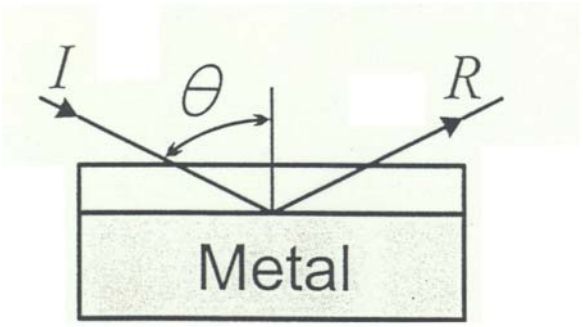

Single (external) reflection

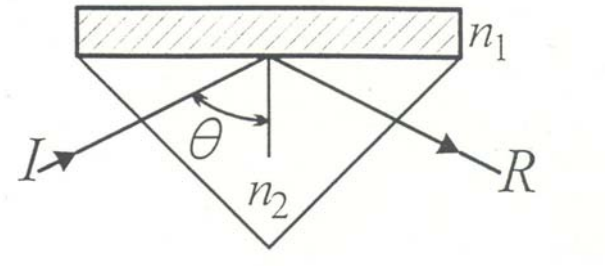

Single (internal) reflection

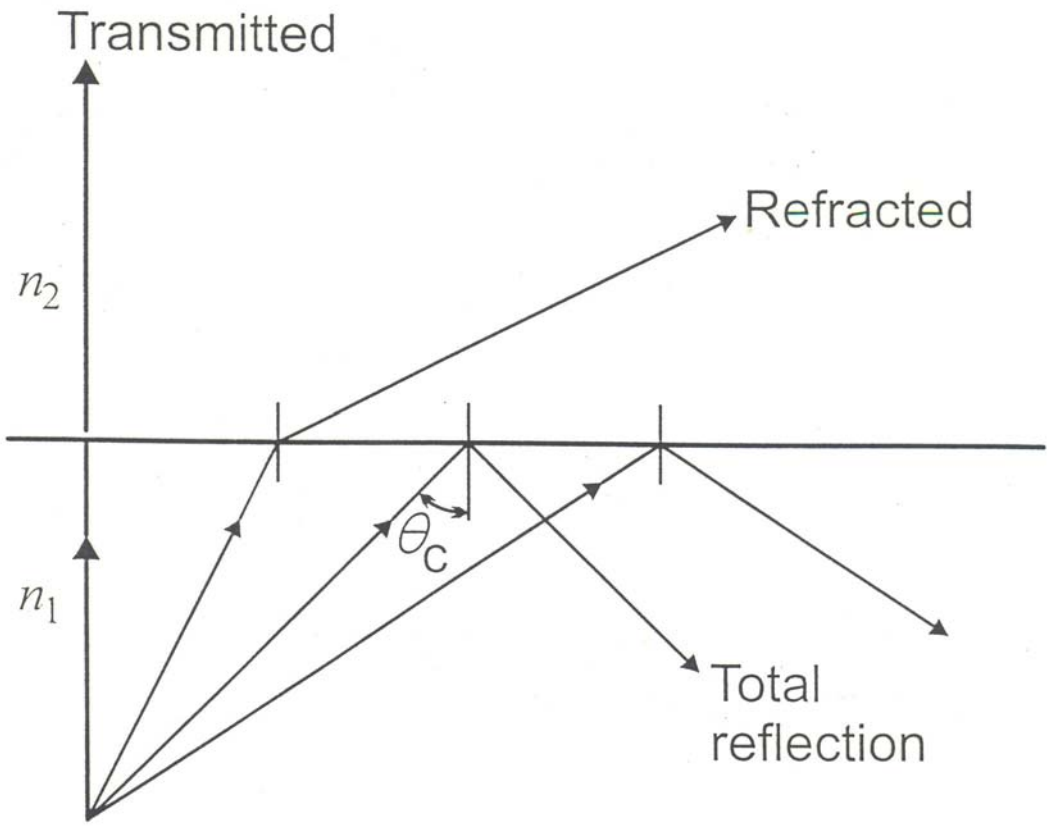

Refractive index changes as a function of incidence angle

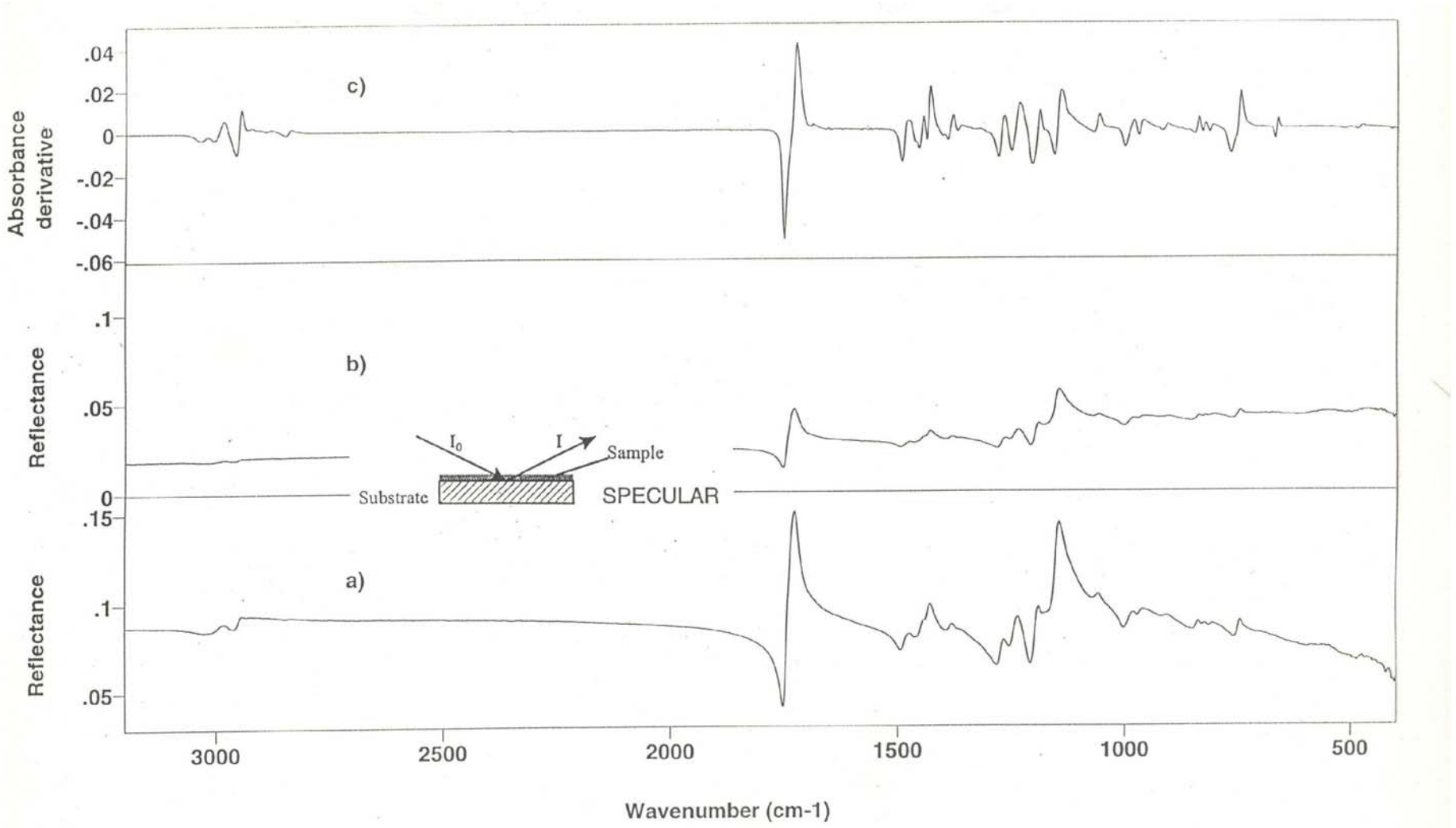

Specular reflectance spectra of a Plexiglas slab compared to derivative absorbance spectrum; (a) reflection from shiny surface, (b) reflection from roughened surface; (c) first derivative of the adsorbance spectrum of PMMA

Total reflection: $\theta > \theta$

$$n_1 \sin \theta_c = n_2 \sin 90°$$

Kramer-Krönig transformation
Quantitative measurement is difficult
Homogeneous sample

2.3. Attenuated total reflection (ATR)

Harrick, Fahrenfort
Optically dense crystal (Si, Ge, KRS5, ZnSe)
The reflectance (R) of the attenuated wave:

$$R = 1 - kd_e$$

d_e – effective layer thickness
k – absorptivity

The energy losses after N-fold reflections

$$R^N = (1 - kd_e)^N$$

The depth of penetration d_p:

$$d_p = \frac{\lambda_0}{p\pi n_1 (\sin^2\theta - n_{21})^{\frac{1}{2}}}$$

λ_0 – wavelength
θ – angle of incident
n_{21} – the refractive index ratio of the sample and crystal

METHODS OF ATR

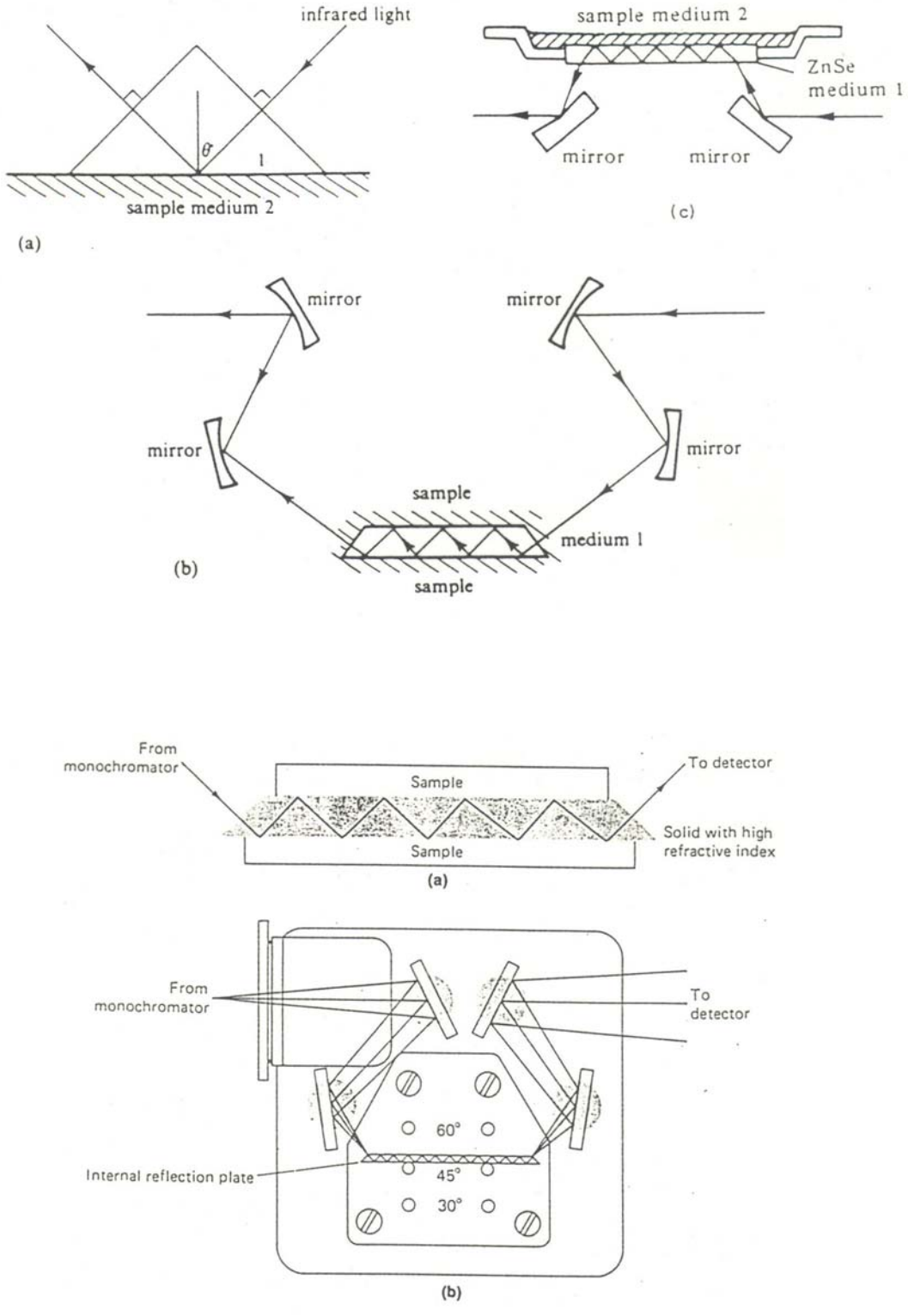

Internal reflectance apparatus

(a) Sample mounted on reflection plate;

(b) Internal reflection adapter

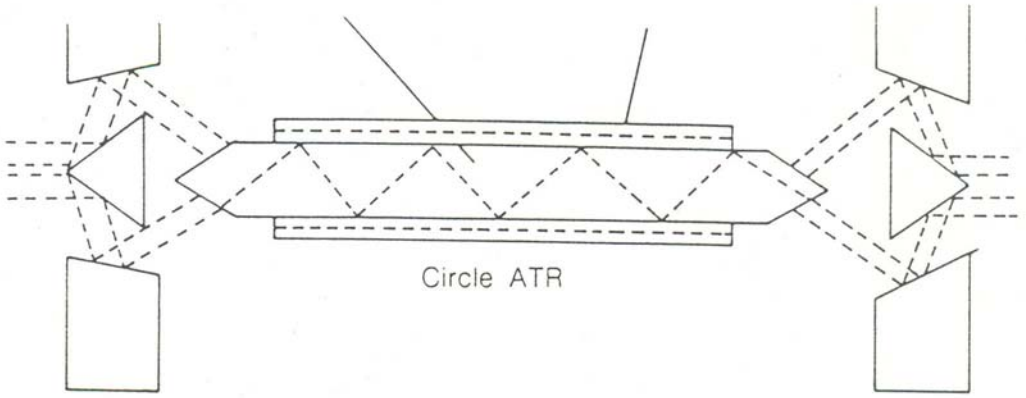

(A)

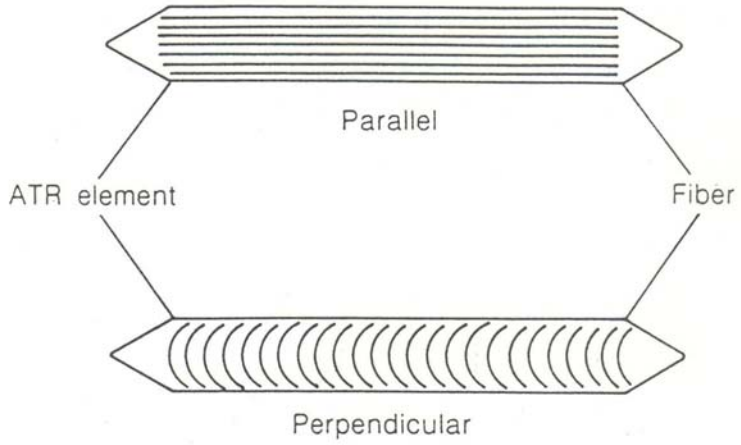

(B)

(A) Circular ATR configuration setup;
(B) Parallel and perpendicular alignment of fibres with respect to a crystal axis

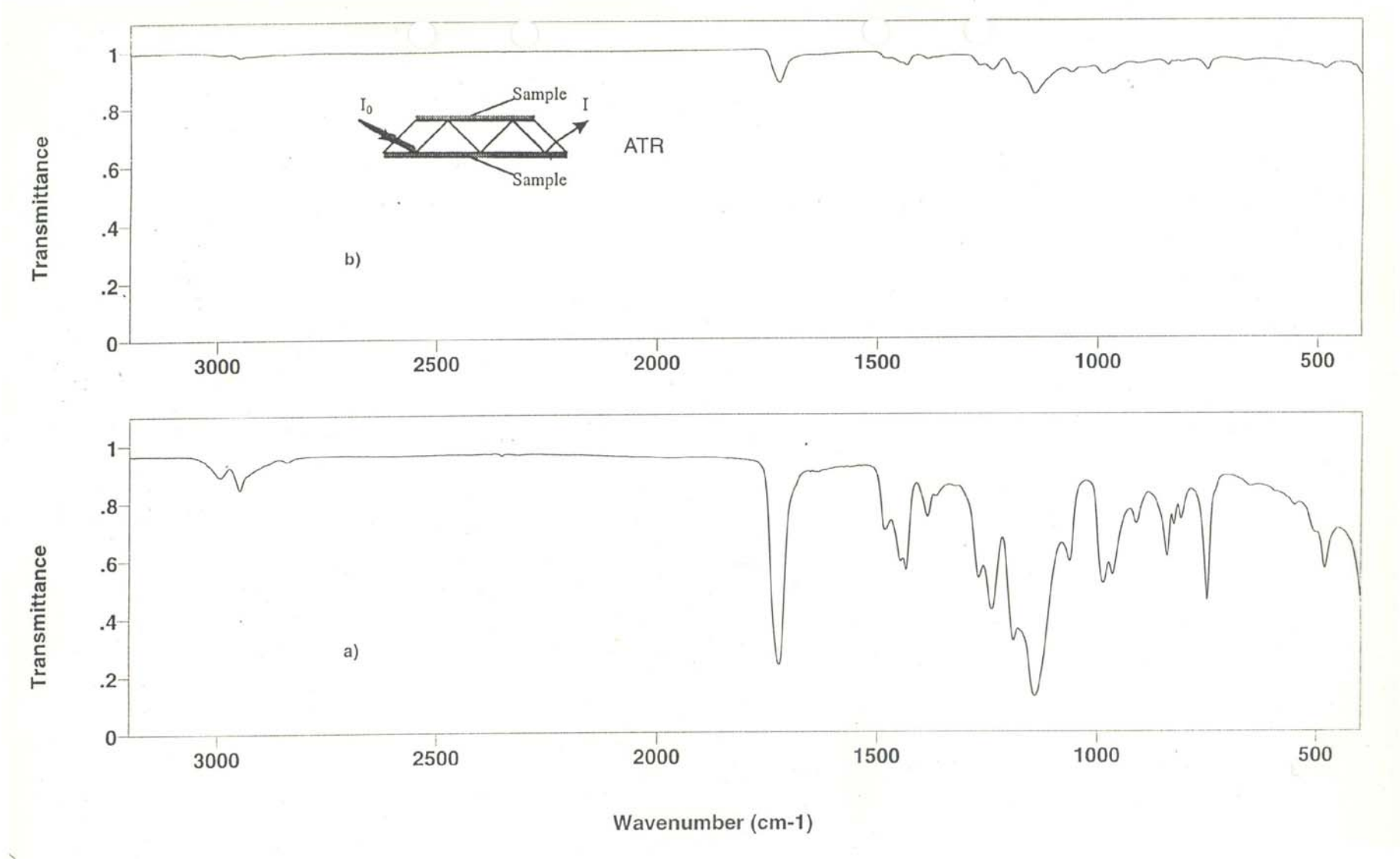

ATR spectra of Plexiglas lab: (a) with shiny surface, (b) with roughened surface

2.4. GRAZING ANGLE REFLECTION

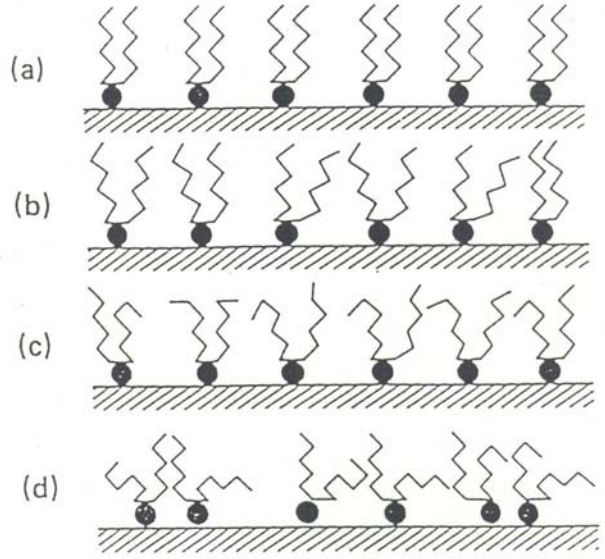

Schematic diagram of the gradual melting process in L-B monolayer of CdA.

(a) ordered room temperature solid; (b, c) gradual disordering of alkyl tails with ordered head group lattice; (d) irreversible breakup of head group lattice

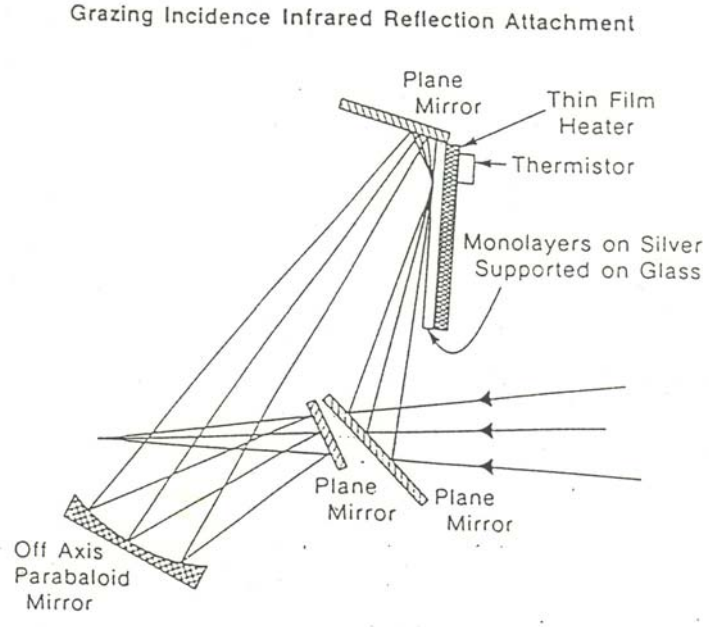

Sample holder for grazing incidence reflection experiments at elevated temperatures

2.5. DIFFUSE REFLECTION (DRIFT)

The diffuse reflectance Fourier transforms spectroscopy (DRIFTS) technique less practiced than the transmission mode, but it is extremely useful, indeed indispensable, for non transparent materials or for *in situ* measurements at elevated temperature.
Any radiation focused on surface can, depending on the characteristic of the surface and its environment, be absorbed, specularly reflected, internally reflected or diffused in all directions. The later effect is of interest in diffuse reflection spectroscopy.

- Kubelka–Munk (1931, 1948)
- UV–VIS, NIR
- Lambert-Beer law in diffuse reflection

$$f_{(R)} = \frac{(1-R_\infty)^2}{2R_\infty} = \frac{K}{s}$$

R_∞ = absolute reflectance of the layer
s = scattering coefficient (particle size dependent)
K = molar absorption coefficient

Quantitative measurements:

$$f_{(R)} = \frac{(1-R_\infty)^2}{2R_\infty} = \frac{c}{k'}$$

c = concentration
k' = $\frac{s}{2.303k}$ (particle size dependent)

FTIR, Fuller, Griffiths (1987)

The diffuse component of the radiation contains data on the absorption properties of the material. This complex radiation contains similar data to those of transmission spectrum. Figure below shows the principle of catalytic cell for DRIFTS measurements.

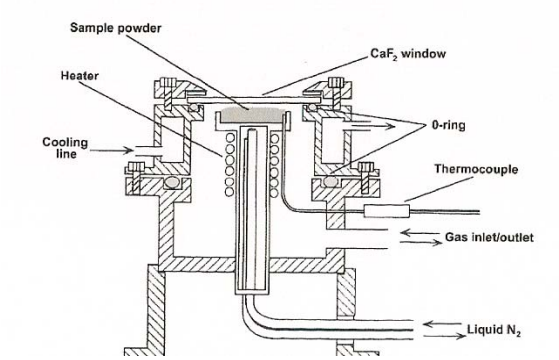

FTIR cell reactor for DRIFTS measurements of catalysts.

This *in situ* cell serves to: subject the sample to reactive conditions; reach temperatures of 1173 K at atmospheric pressure or 673 K at 100 bar; record the sample spectra at elevated temperatures; directly control the sample temperature in intimate contact with the catalyst powder.
The sample holder, a ceramic crucible attached to the heating resistor and a thermocouple, is placed inside the catalytic chamber with CaF_2, BaF_2 or ZnSe windows. See the real picture of the cell in Figure below.

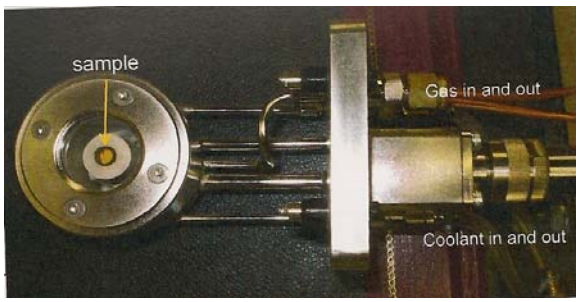

The DRIFTS technique offers the advantages of simple sample preparation, the capacity to analyze non transparent, dark and black colored samples, irregular surfaces, exposure of the sample to simulated reaction conditions, while recording of the spectrum of the catalyst at elevated temperature under pressure.
Successful applications of DRIFTS for *in situ* measurements of catalysts have been described in a few review papers.

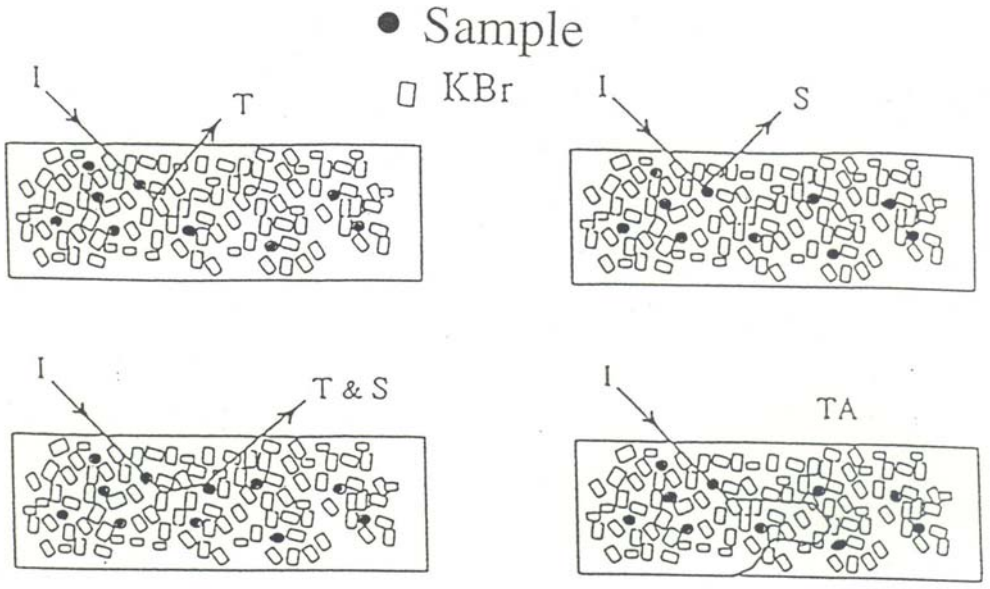

Mixed reflection modes are shown in DRIFTS measurements. In these diagrams the possible paths of the incident beam (I) are shown that can produce transmission (T) spectra, specular reflection (S) spectra, and total absorption (TA)

DRIFT OPTICAL ARRANGEMENT

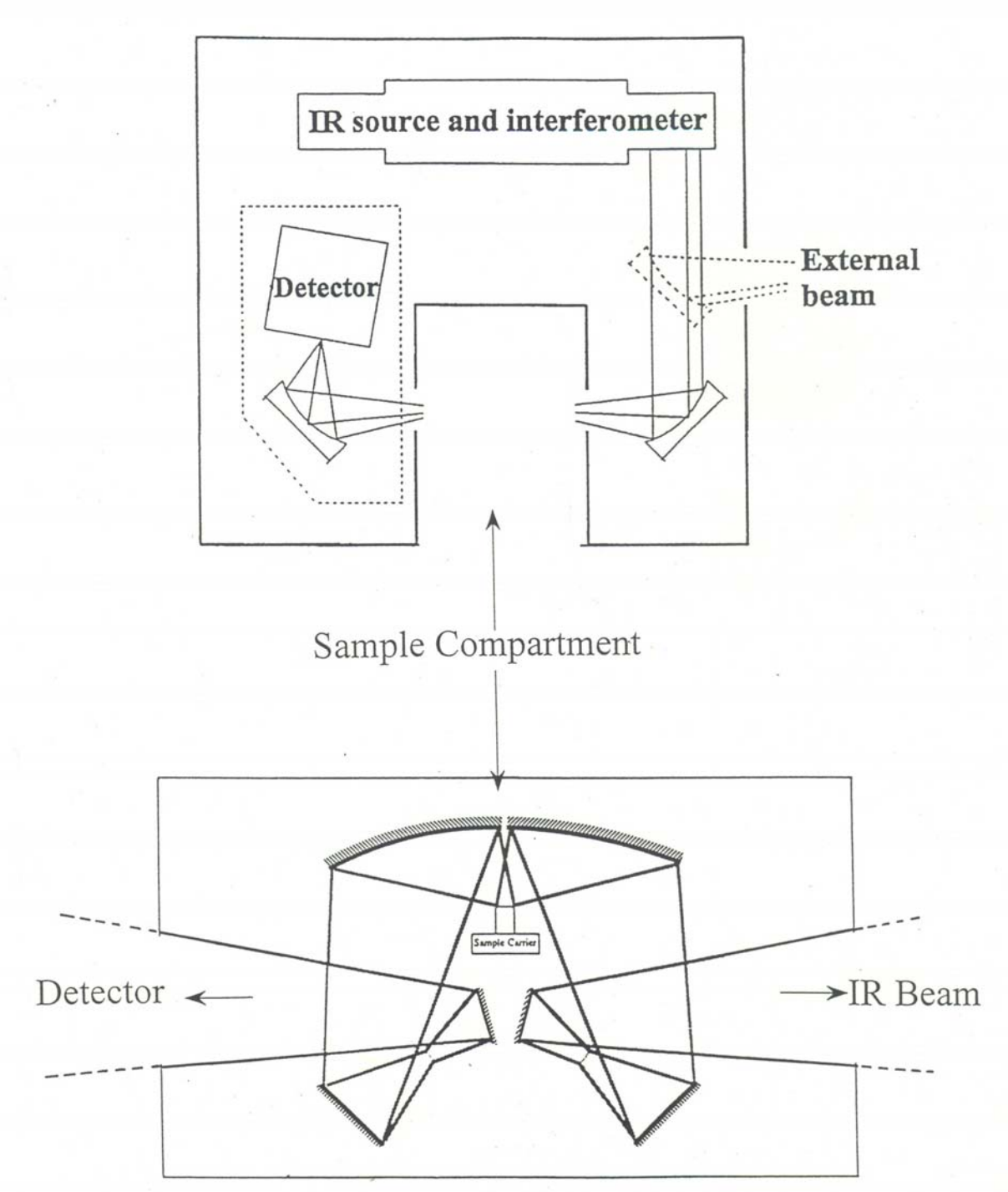

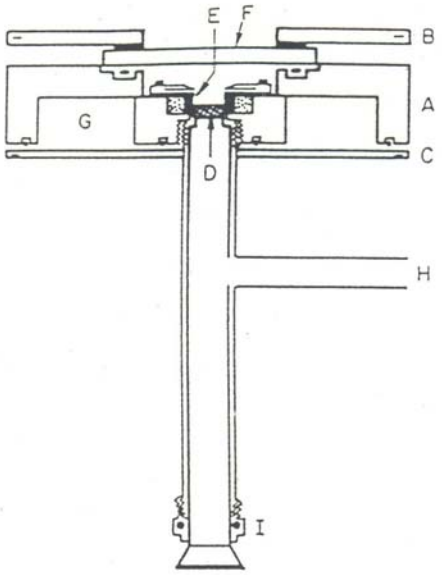

Diffuse reflectance cell.

A: Main body;
B: Coverplate for sample compartment;
C: Coverplate for the cooling water cavity;
D: Frit to support the sample;
E: Sample heater;
F: KCl window;
G: Cavity for cooling water ;
H: Gas outlet line;
I: Nut to vacuum tighten the sample holder to the housing tube

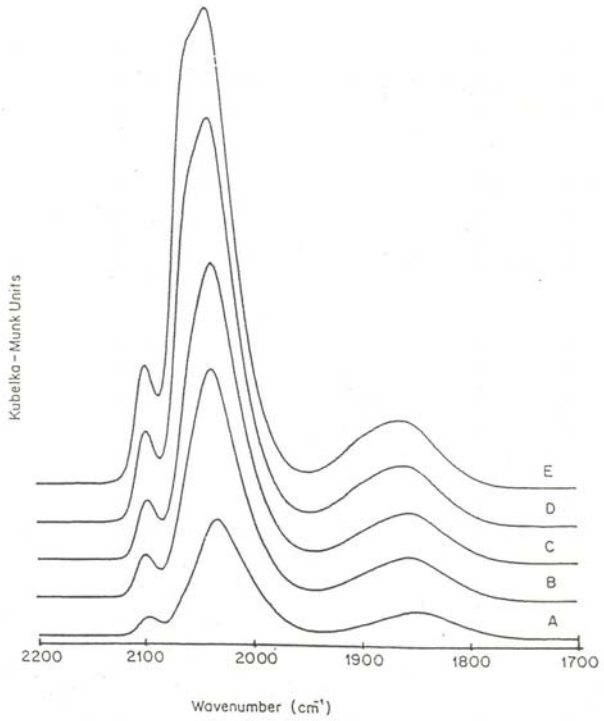

DR spectra of CO on 1% Rh/Al_2O_3 at equilibrium pressures above 0.1 torr,
(A) 0.204torr; (B) 0.502 torr; (C) 1.26 torr; (D) 3.50 torr; (E) 8.42 torr

Difference of DRIFT spectra of $[Re(CO)_3OH]_4$ on Al_2O_3 (1.5% Re) and of Al_2O_3 (both samples were 1.5% mixture with KBr

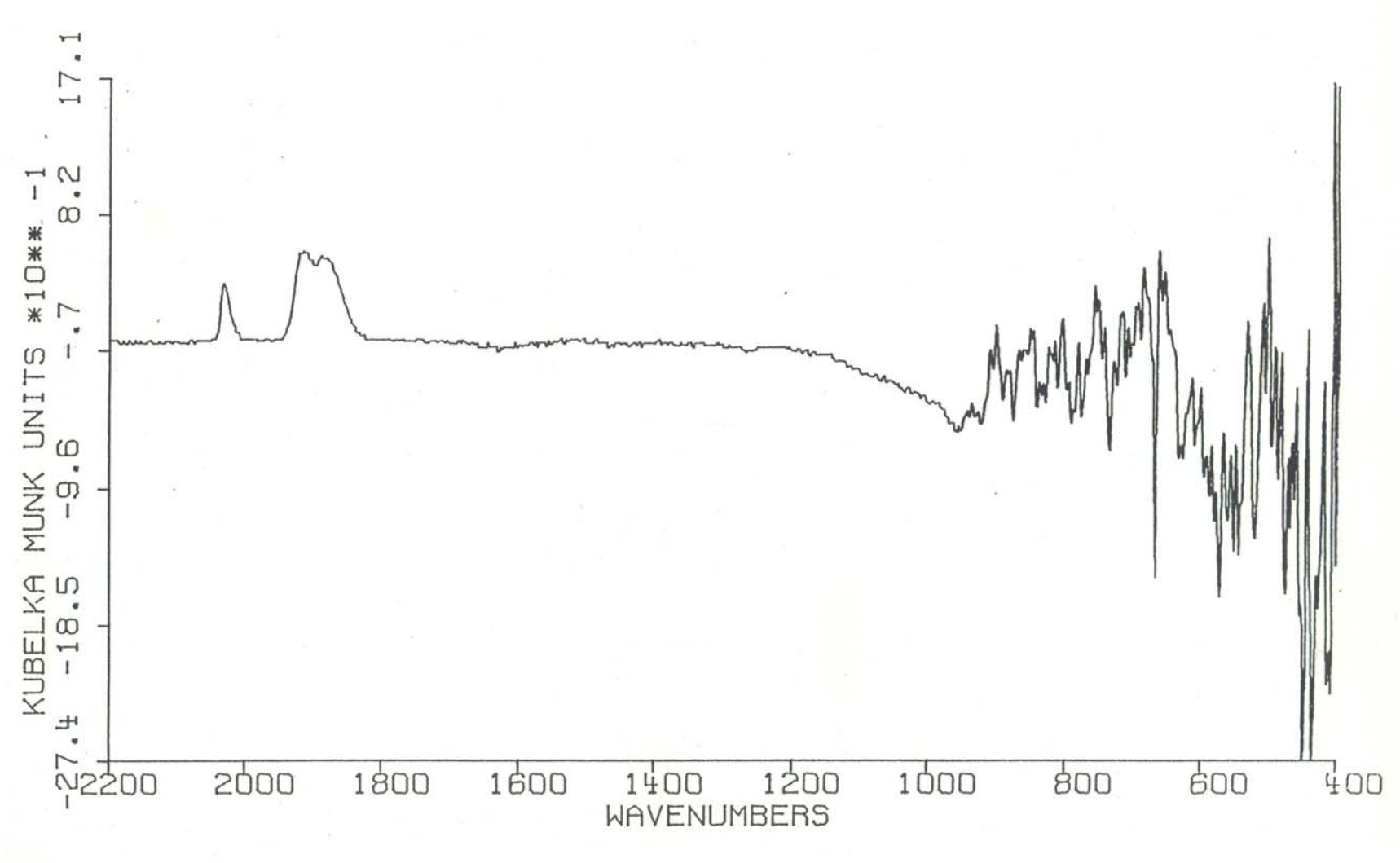

Difference spectrum (SiO_2)subtracted)

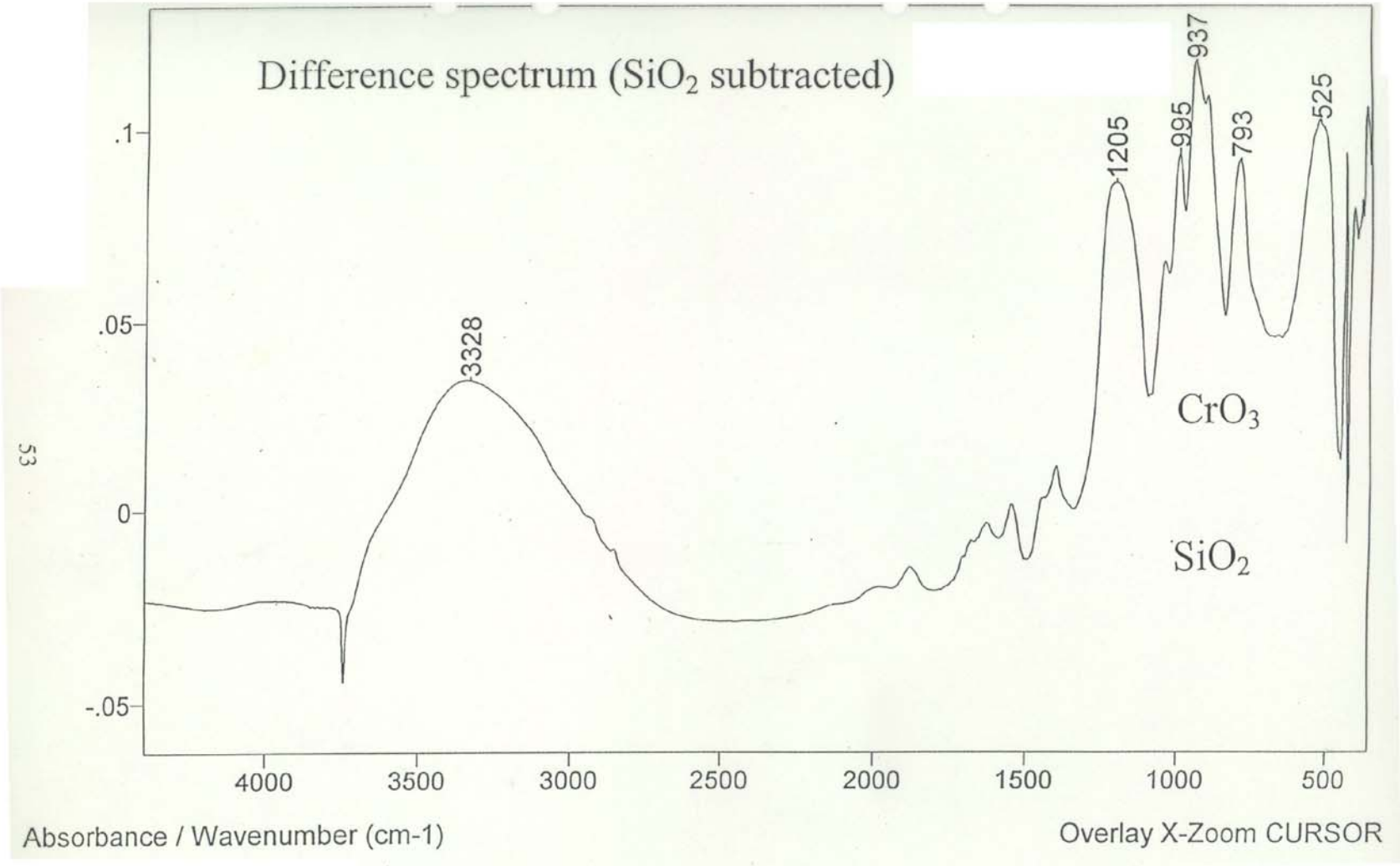

2.6. PHOTOACOUSTIC SPECTROSCOPY (PAS)

The photoacoustic phenomenon was invented as early as 1880 by Alexander Graham Bell, while experimenting with a photo phone. After this accident discovery however the phenomenon remained in the background until the advent of microphone.
Photoacoustic (PA) signals are unique in that they depend directly on the energy absorbed by the sample, rather than on what is transmitted or reflected. The sample is placed in a sealed chamber (Figure below).

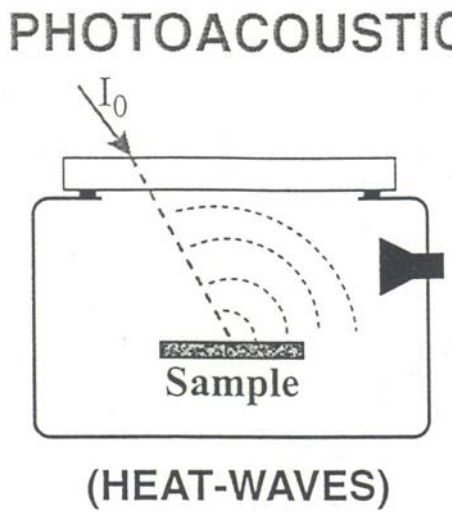

- Modulated incident light
- Heat generation in the sample
- Temperature fluctuation at the surface
- Pressure changes in the gas phase (He)
- Detector= microphone

Generation of the signal:

I_0 = modulates incident radiation
n – refractive index of the sample
β – absorption coefficients
I(x) – intensity of light at depth x:

$$I(x) = I_0 (1-n) \exp(-\beta x)$$

The amount of light adsorbed within the thickness x is equal to

$$E(x) = \beta I(x) = \beta I(1-n) \exp(-\beta x)$$

The depth of optical penetration is defined as optical adsorption length, L_β and is inversely proportional to β:

$$L_\beta = \frac{1}{\beta}$$

The efficiency of the heat transfer is determined by the **thermal diffusion coefficient a_s** and the modulation frequency **ω**

$$a_s = \left[\frac{\omega}{2\alpha}\right]^{1/2}$$

α – thermal diffusivity

The thermal diffusion length μ_{th}

$$a_{th} = \frac{1}{a_s}\left[\frac{2\alpha}{\omega}\right]^{1/2}$$

PA signal:

- optical
- thermal

} Properties of the sample

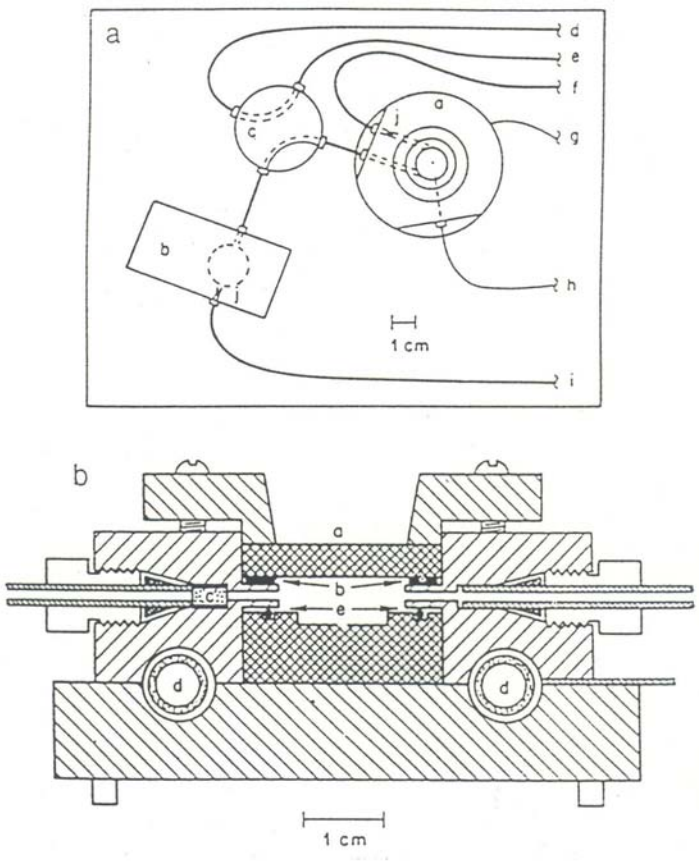

(a) Photoacoustic spectroscopy sample cell and microphone chamber.

a. sample cell; b, microphone chamber; c, isolation valve; d, microphone chamber outlet; e, sample cell inlet; f, sample cell outlet; g, sample heater power line; h, thermocouple; i, microphone chamber inlet; j, 5 m stainless-steel frit

(b) High temperature photoacoustic spectroscopy cell

a, KBr window; b, 0.8 mm graphite gasket; c, 5 m stainless-steel frit; d, spiral electric heater; e, hollow metal O-ring

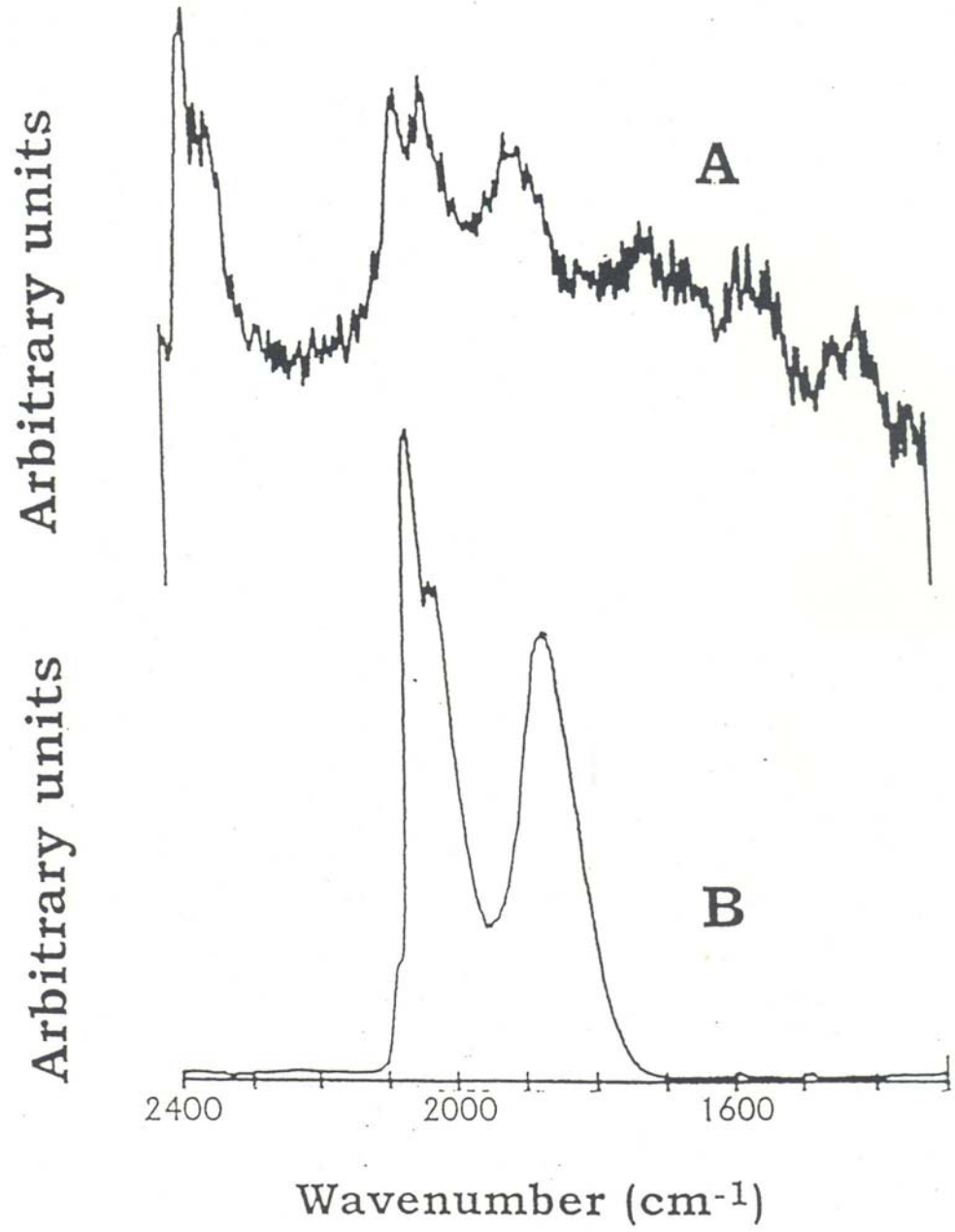

(A) Photoacoustic spectrum of CO adsorbed on 5% Rh/Al_2O_3 (1024 scans)

(B) DR spectrum (in Kubelka-Munk format) of the same catalyst treated in the same manner as for Figure (1 scan)

Typical photoacoustic Fourier transform infrared (FTIR-PAS) setup for analysis of solid and liquid samples contains an interferometer, a focusing mirror, and a photoacoustic cell (Figure 30). FTIR interferometer consists of a beamsplitter and two mirrors. The infrared beam is split into two beams: one is reflected from a fixed mirror and one from a moving mirror. By combining the two beams each wavelength of the light is modulated with a different modulation frequency. The combined beam is then focused into the solid or liquid sample in the photoacoustic cell. The generated photoacoustic signal can be directly transformed into absorption spectrum.
Depth-varying information of the sample can be obtained by varying the mirror velocity or phase angle of detection. Typically for solid materials the depth from where the spectra are obtained can be varied from few micrometers to about 100 micrometers.

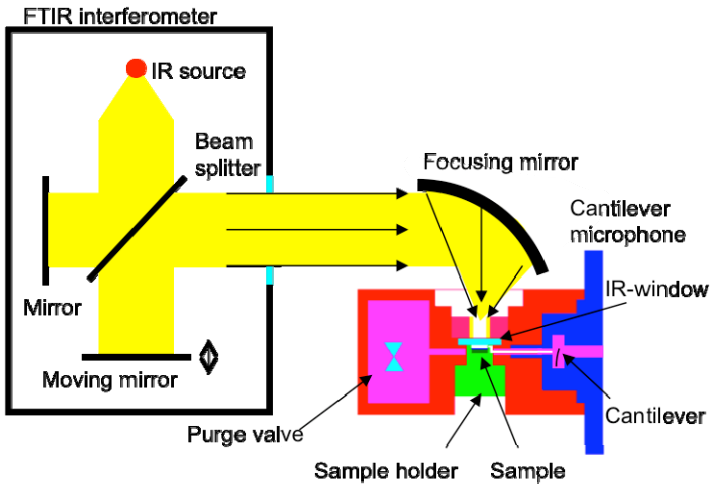

Typical photoacoustic Fourier transform infrared (FTIR-PAS) setup for analysis of solid and liquid samples.

The FTIR analysis of solid- and liquid-phase samples has a great variety of applications and advantages compared to other techniques. The most important and best-known advantages are:

- minimal sample preparation required,
- suitability for opaque materials,
- possibility for depth profiling,
- non-destructive measurement, which means that the sample is not consumed.

The typical applications of solid- and liquid-phase photoacoustic FTIR are the study of

- carbons,

- coals,
- hydrocarbons,
- hydrocarbon fuels,
- corrosion,
- clays and minerals,
- wood and paper,
- polymer layers,
- food products,
- biology and biochemistry e.g. proteins, bacteria and fungi,
- medical applications such as human tissue,
- drug characterization and penetration,
- teeth, hair and bacteria,
- and non-destructive measurement of carbonyl compounds, textiles, and catalysts.

Due to the ultra-high sensitivity of the Gasera (Turku, Finland) novel cantilever sensor, high quality spectra can be obtained in just seconds unlike in other available photoacoustic accessories. In fact the PA301 is over **100x faster** that other competing PA solutions in the market. Furthermore, ambient air can be used as the carrier gas to obtain a signal-to-noise ratio (SNR) that is still significantly better compared to other commercial photoacoustic detectors used with helium carrier gas.

New FTIR Photoacoustic accessory PA301, based on very sensitive cantilever sensor.

2.7. IR REFLECTION-ABSORPTION SPECTROSCOPY (IRAS OR RAIRS)

ADSORPTION ON METAL SURFACES

- Atoms and molecules can form **chemical** bonds to metal surfaces ("chemisorptions"). Typical chemisorptions' energies: ~ 0.4 - 2.0 eV molecule^{-1} (~40 - 200 kJ mol^{-1})

- Bond energies below 0.4 eV molecule-1 are symptomatic of **physisorption**

- Chemisorption is **selective** with respect to the metal surface and its orientation

- On single crystal surfaces adsorbates take up specific surface sites and often form **ordered** over layers indicative of strong **lateral interactions**

- Chemisorption bond formation is expected to modify the **electronic structure** and **vibrational properties** of the adsorbates (and of the substrate surface)

- **VIBRATIONAL SPECTROSCOPY**
    - High resolution electron energy loss spectroscopy (HREELS)
    - IR reflection-absorption spectroscopy (IRAS or RAIRS)
    - Surface-enhanced Raman spectroscopy (SERS)
    - Helium atom scattering
- **Photoabsorption**
    - Near edge X-ray absorption fine structure (NEXAFS or EXAFS)
    - Extended absorption fine structure (surface EXAFS): a structural tool
- **Photoelectron spectroscopy**
    - Core level photoemission (XPS); photoelectron diffraction: also a structural tool
    - Valence level photoemission (UPS)

Cu{111}

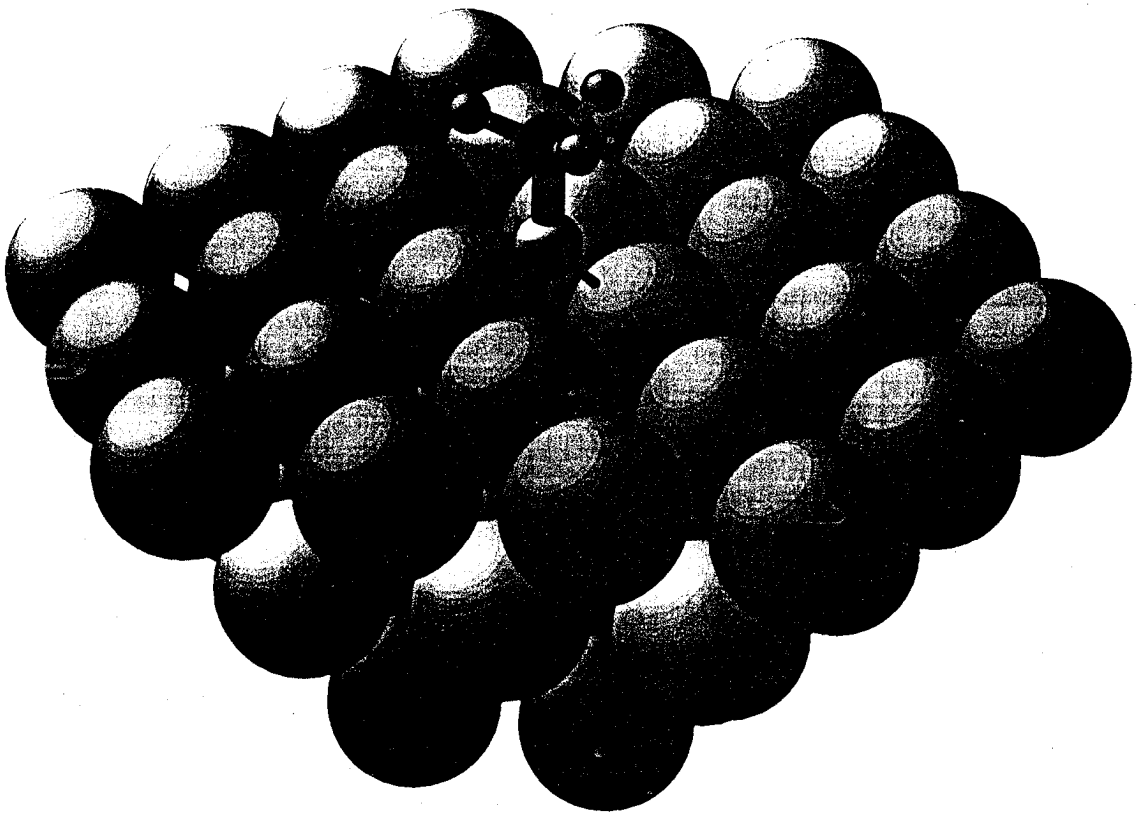

$$2\ CH_3OH + O \rightarrow 2\ CH_3O + H_2O\uparrow$$

Ni{111}

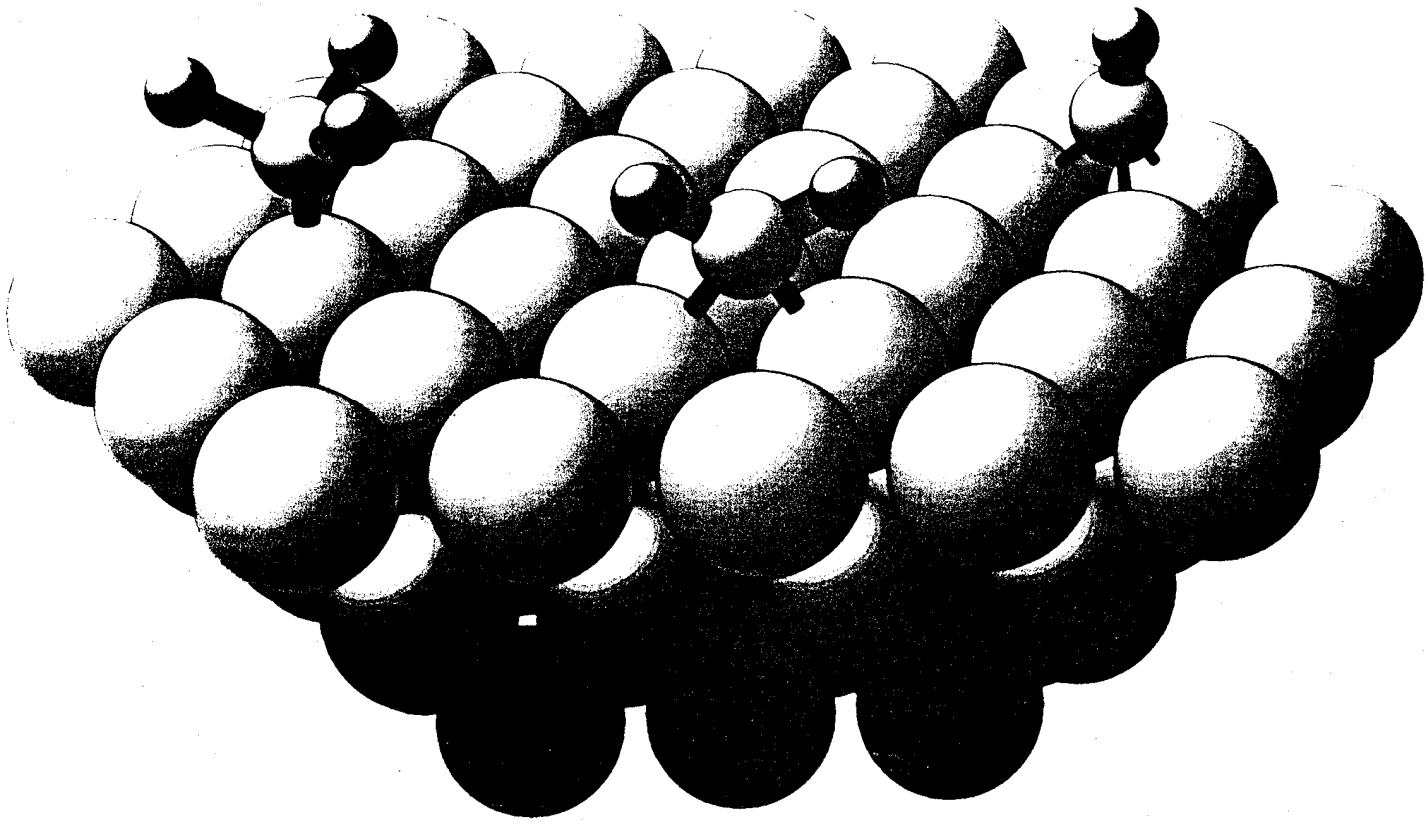

$$PF_3 \xrightarrow[h\,\nu]{e^- \text{ or}} PF_3, PF_2, PF$$

Cu{110}

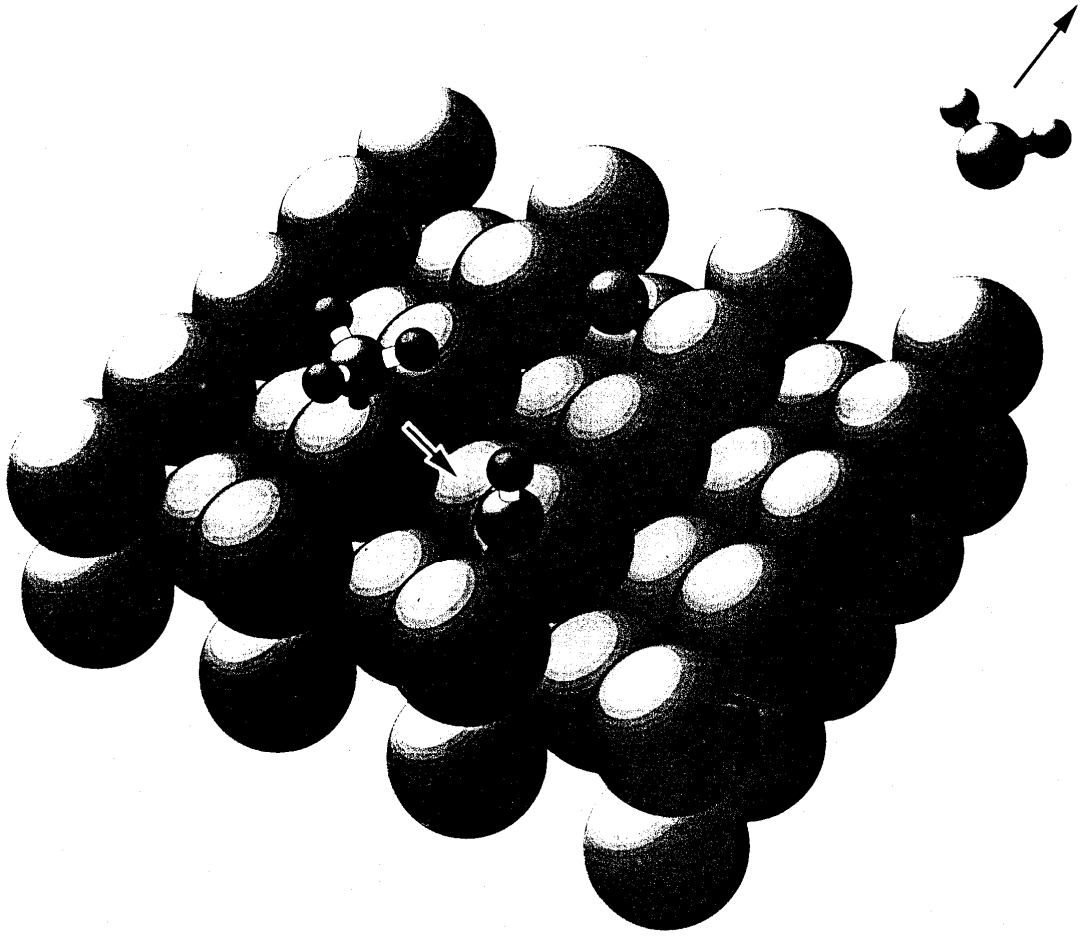

$$NH_3 + O \rightarrow NH + H_2O\uparrow$$

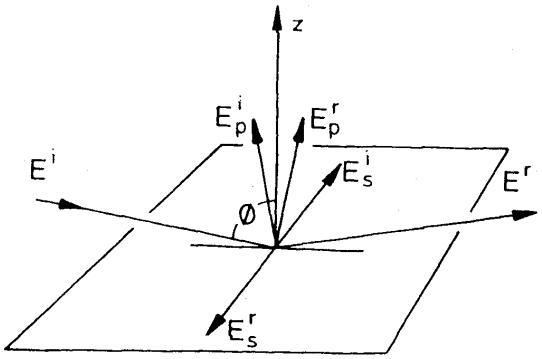
z
E_p^i
E_p^r
E^i
E_s^i
E^r
Ø
E_s^r

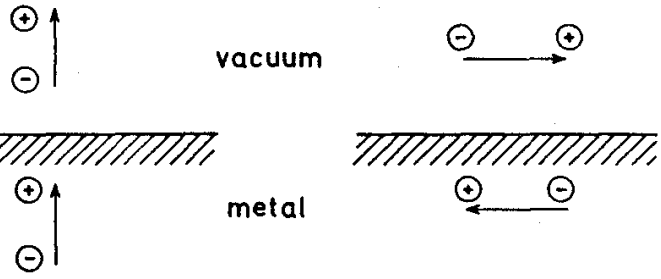
vacuum
metal

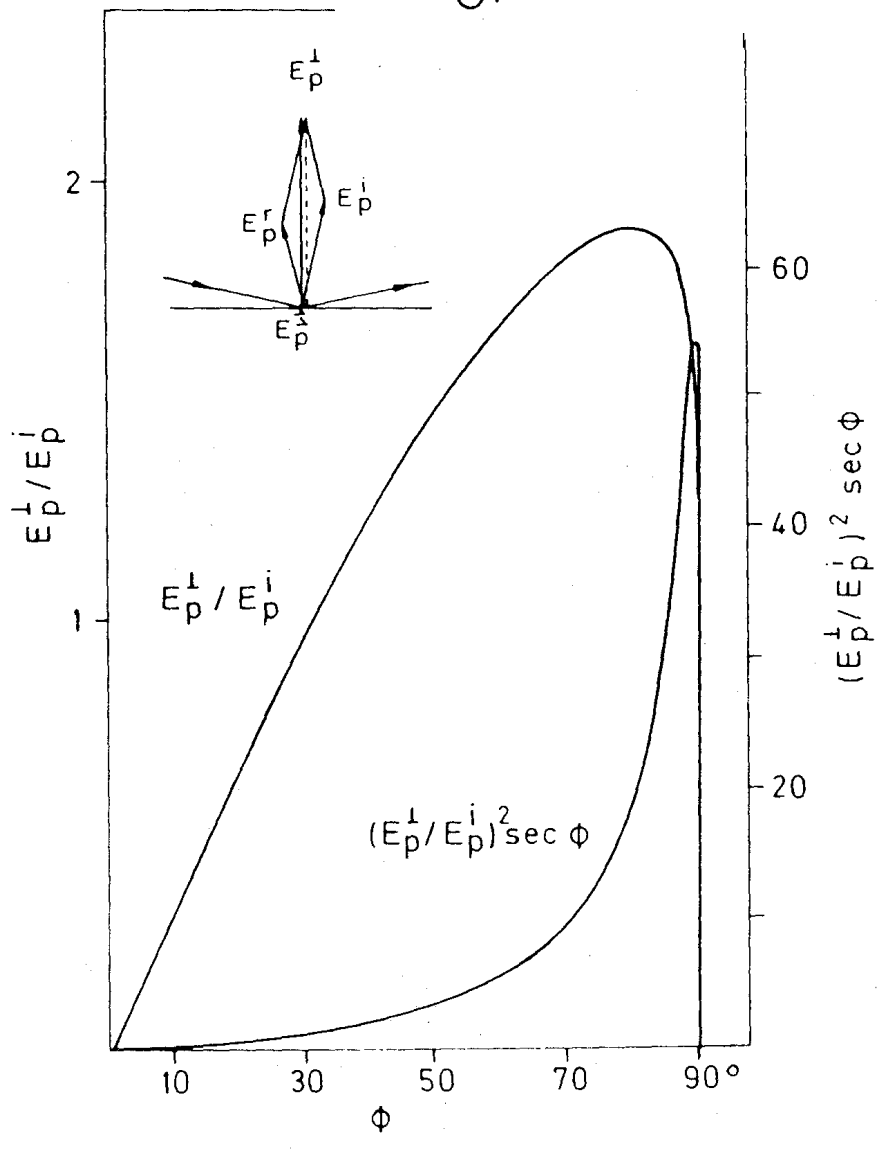
$E_p^\perp$
E_p^r
E_p^i
$E_p^\perp$
2
1
$E_p^\perp / E_p^i$
$E_p^\perp / E_p^i$
$(E_p^\perp / E_p^i)^2 \sec \Phi$
60
40
20
$(E_p^\perp / E_p^i)^2 \sec \Phi$
10
30
50
70
90°
Φ

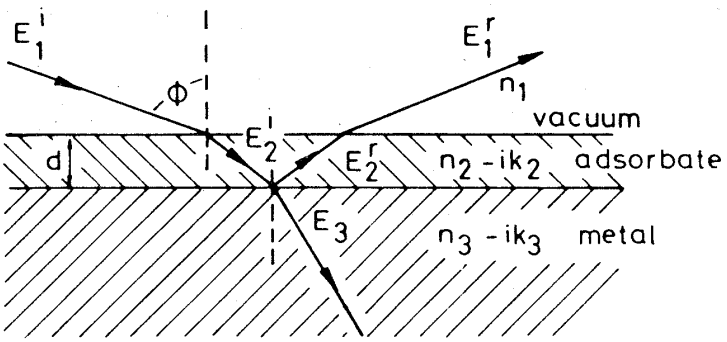
E_1^i
E_1^r
Φ
n_1
vacuum
E_2^i
E_2^r
d
$n_2 - ik_2$
adsorbate
E_3
$n_3 - ik_3$
metal

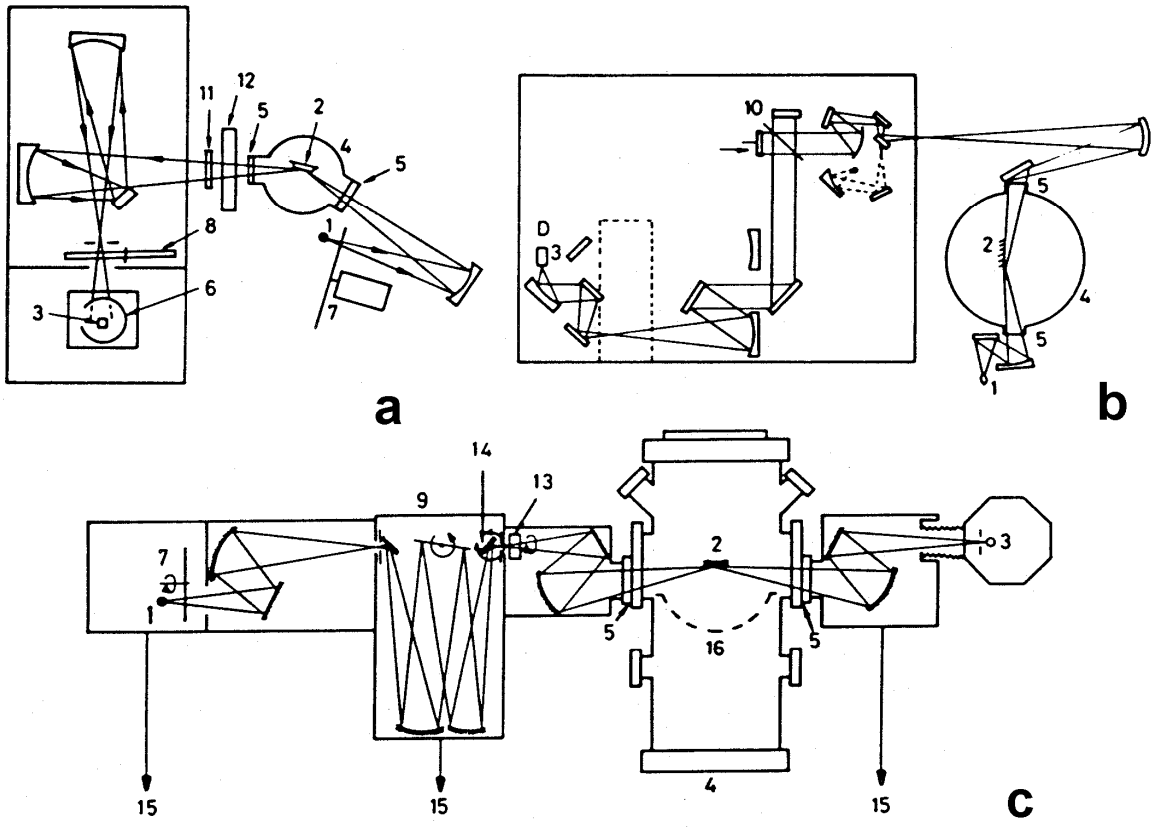
a
b
c

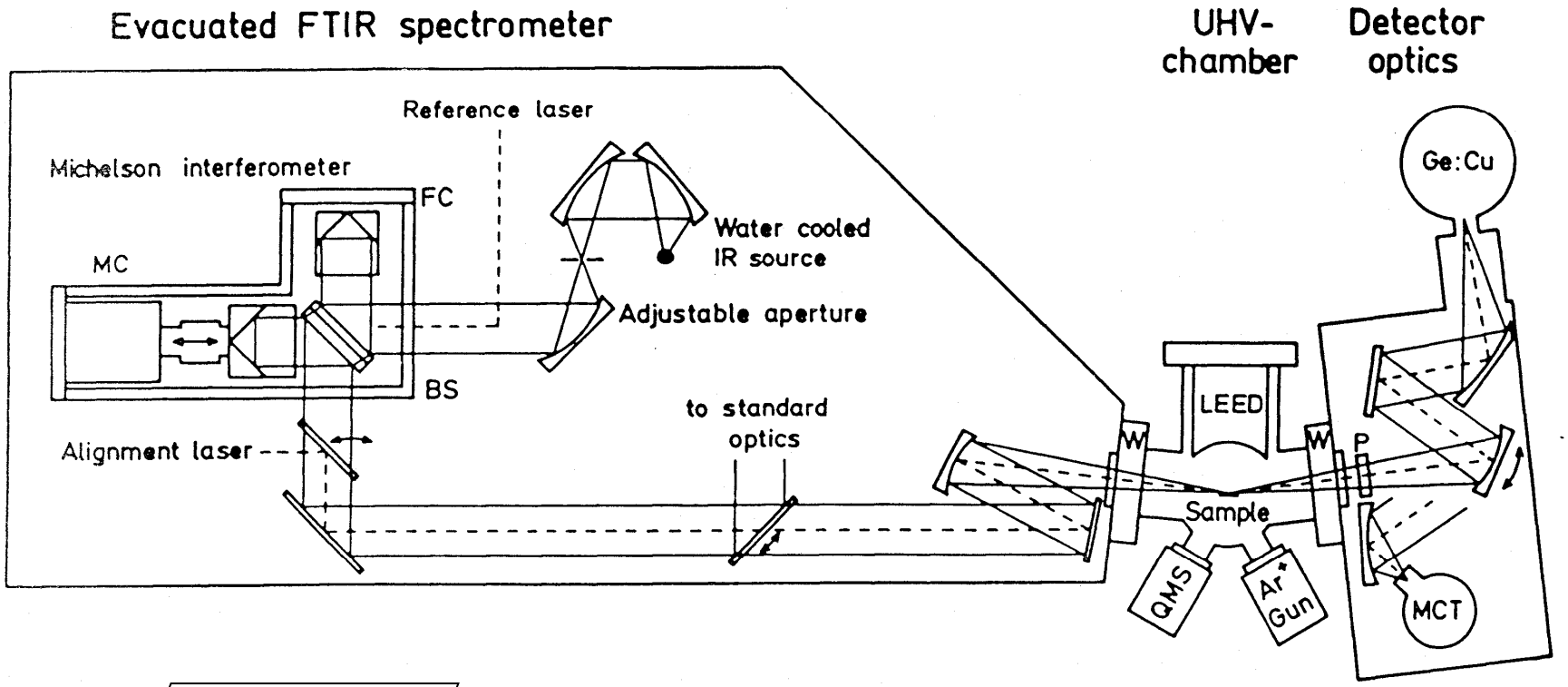

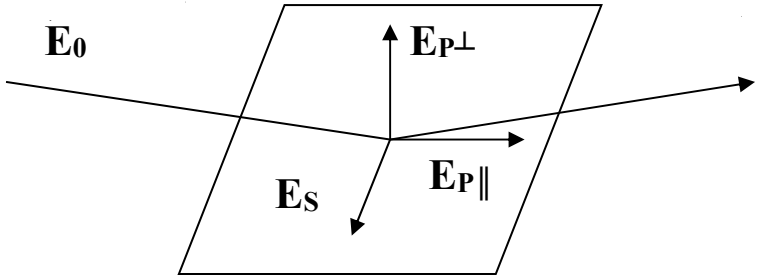

The strong screening effect of the metal surface prevents the parallel electric field components E_S and $E_{p\parallel}$ from building up

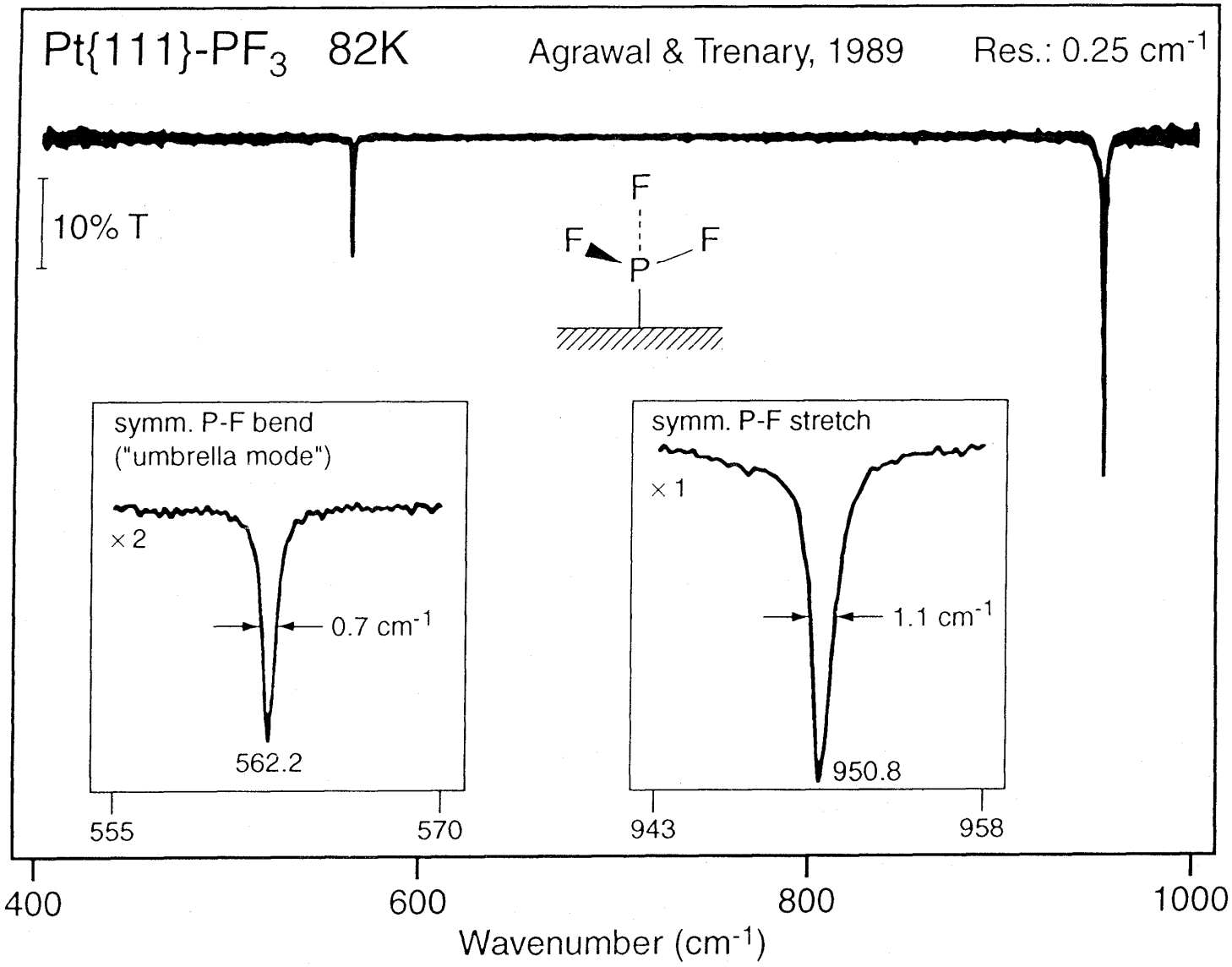
Pt{111}-PF3 82K
Agrawal & Trenary, 1989
Res.: 0.25 cm-1
10% T
F
F
F
P
symm. P-F bend
("umbrella mode")
×2
0.7 cm-1
562.2
555
570
symm. P-F stretch
×1
1.1 cm-1
950.8
943
958
400
600
800
1000
Wavenumber (cm-1)

P. Gardner (UMIST)
J. Miners (FHI)

THE CO/NO OSCILLATORY REACTION ON Pt{100}

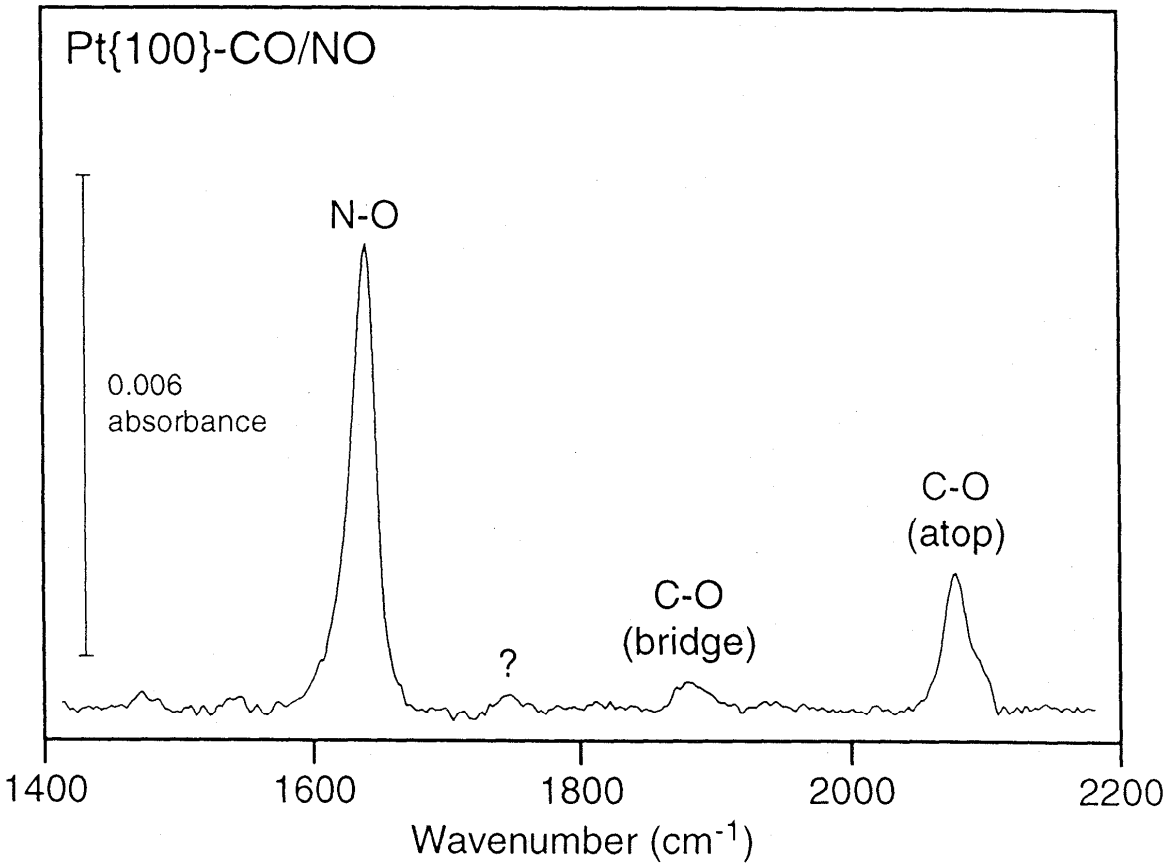

$$NO \rightarrow N_{ad} + O_{ad}$$
$$CO_{ad} + O_{ad} \rightarrow CO_2$$
$$2N_{ad} \rightarrow N_2$$

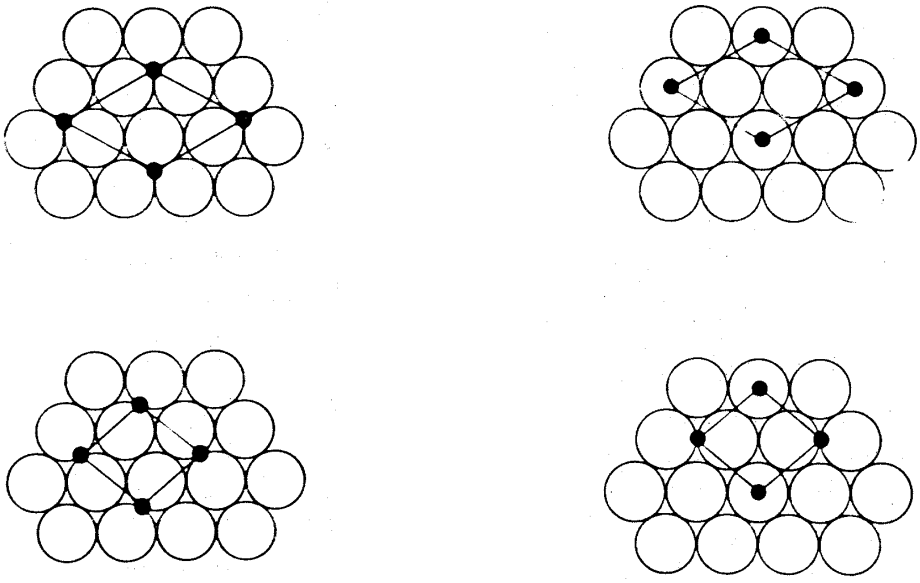

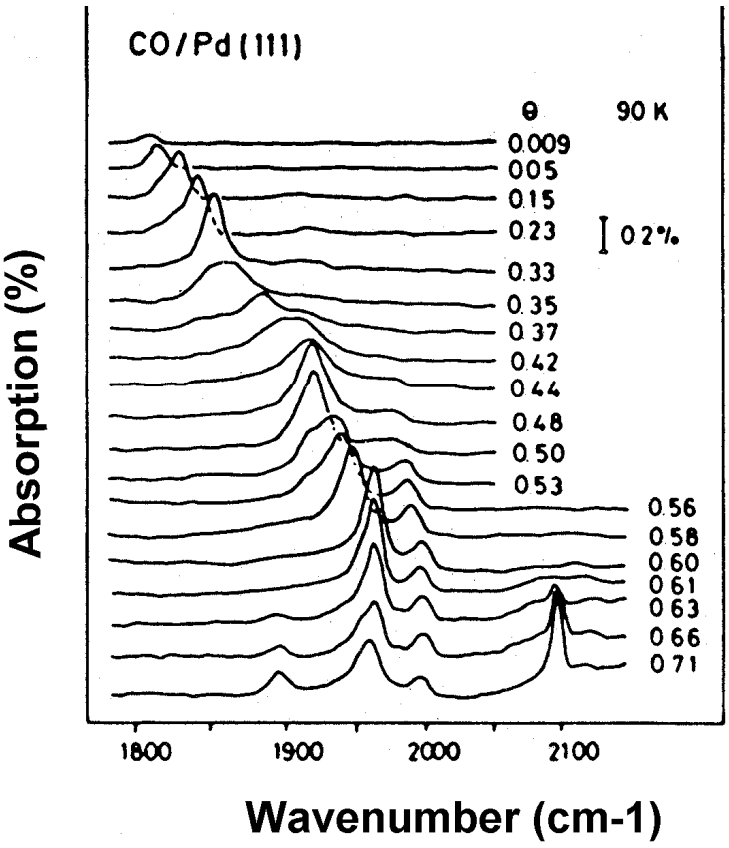
CO/Pd(111)
θ
90 K
0.009
005
0.15
0.23
0.2%
0.33
0.35
0.37
0.42
0.44
0.48
0.50
0.53
0.56
0.58
0.60
0.61
0.63
0.66
0.71
Absorption (%)
1800
1900
2000
2100
Wavenumber (cm-1)

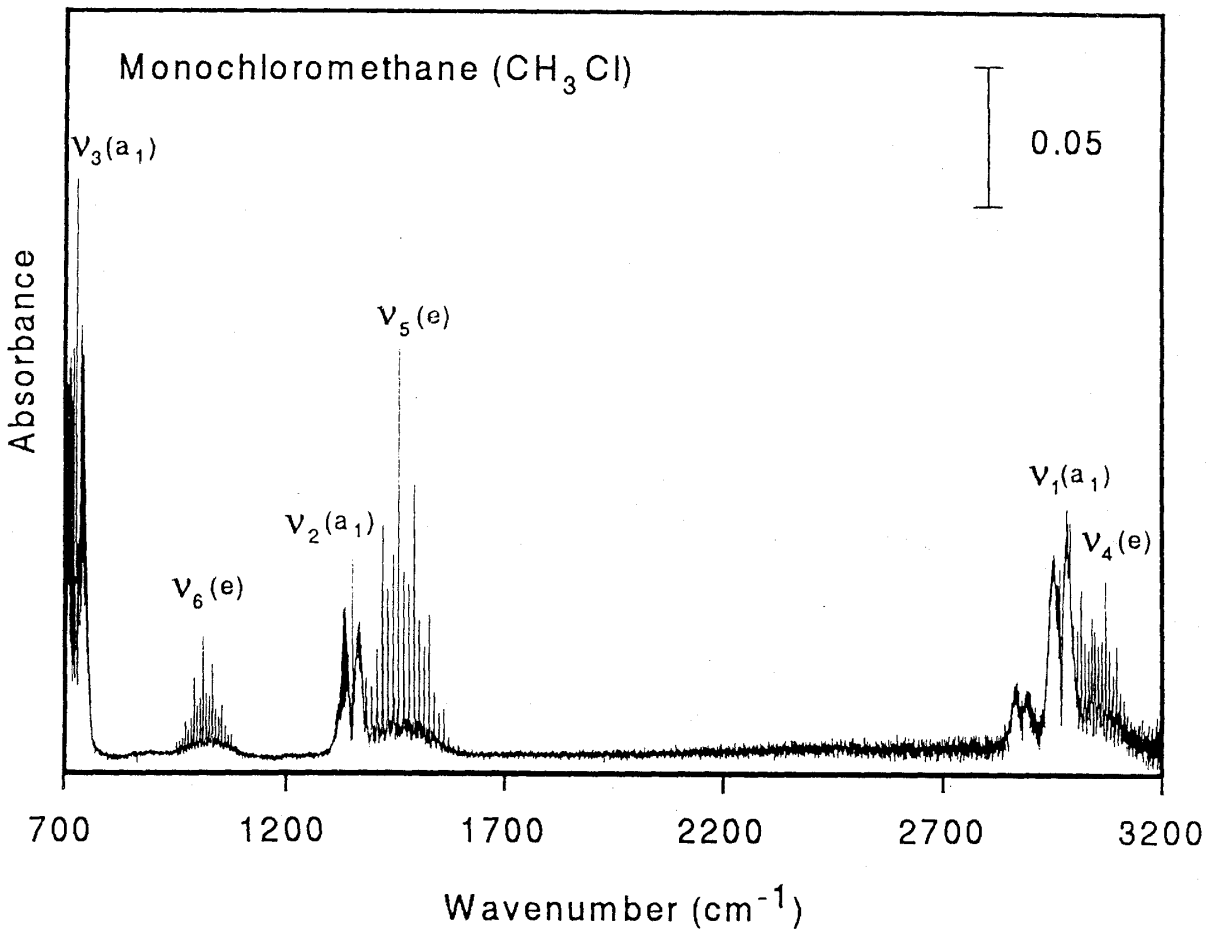
Monochloromethane (CH_3Cl)
0.05
$\nu_3(a_1)$
$\nu_5(e)$
$\nu_2(a_1)$
$\nu_6(e)$
$\nu_1(a_1)$
$\nu_4(e)$
Absorbance
700
1200
1700
2200
2700
3200
Wavenumber (cm^{-1})

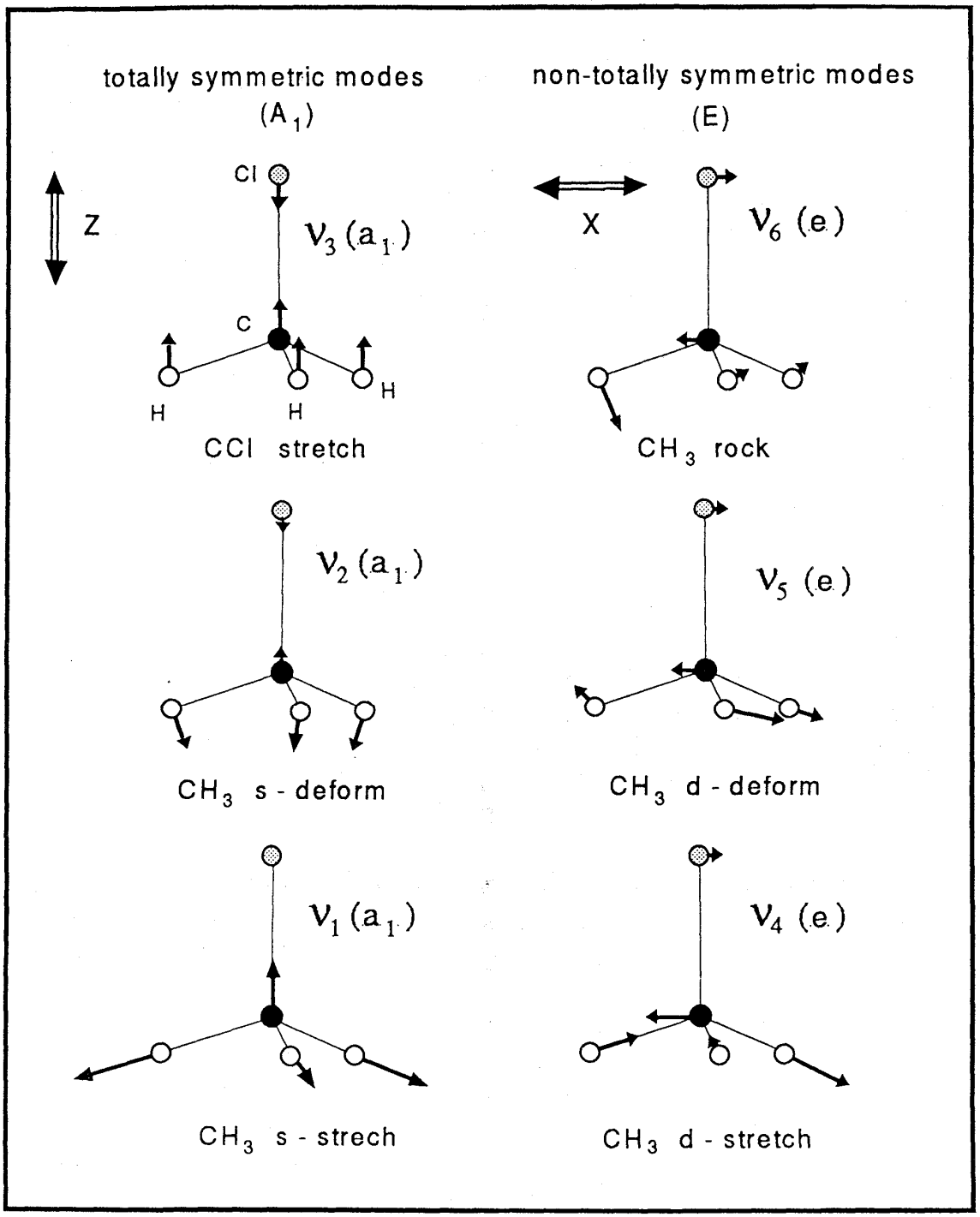

ALL OF THE NINE NORMAL VIBRATIONS OF $CH_3Cl(C_{3v}$ SYMMETRY) ARE IR ACTIVE

K. Knorr (Saarbrücken)
R. Nalezinski (FHI)